One gene - two proteins: The C-terminus of the prototypical M2 muscarinic receptor localizes to the mitochondria and regulates cell respiration.

Irene Fasciani[1†], Francesco Petragnano[1†], Ziming Wang[2], Ruairidh Edwards[3], Narasimha Telegu[2], Ilaria Pietrantoni[1], Ulrike Zabel[4], Henrik Zauber[2], Marlies Grieben[2], Maria E. Terzenidou[3], Jacopo Di Gregorio[1], Cristina Pellegrini[1], Silvano Santini Jr[5], Anna R. Taddei[6], Barbel Pöhl[2], Stefano Aringhieri[7], Marco Carli[7], Gabriella Aloisi[1], Francesco Marampon[8], Eve Charlesworth[9], Alexandra Roman[2], Sebastian Diecke[2], Vincenzo Flati[1], Franco Giorgi[7], Fernanda Amicarelli[5], Andrew B. Tobin[3], Marco Scarselli[7], Kostas Tokatlidis[3], Mario Rossi[1], Martin J. Lohse[2,4,10]*, Paolo Annibale[2,9]*, Roberto Maggio[1]*

[1] Department of Biotechnological and Applied Clinical Sciences, University of L'Aquila, 67100 L'Aquila, Italy.
[2]Max Delbrück Center for Molecular Medicine, 13125 Berlin, Germany.
[3]Centre for Translational Pharmacology, Institute of Molecular, Cell and Systems Biology, College of Medical, Veterinary and Life Sciences, University of Glasgow, G128QQ Glasgow, UK.
[4]Institute of Pharmacology and Toxicology, University of Würzburg, 97078 Würzburg, Germany.
[5]Department of Life, Health and Environmental Sciences, University of L'Aquila, 67100 L'Aquila, Italy.
[6]Section of Electron Microscopy, Great Equipment Center, University of Tuscia, Viterbo, Italy.
[7]Department of Translational Research and New Technology in Medicine, University of Pisa, 56126 Pisa, Italy.
[8]Department of Radiotherapy, University of Roma La Sapienza, 00151 Roma, Italy.
[9]School of Physics and Astronomy, University of St Andrews, KY16 9SS St Andrews.
[10]ISAR Bioscience Institute, 82152 Munich, Germany.
[†] Equal contribution
*email: martin.lohse@isarbioscience.de;
*email: roberto.maggio@univaq.it;
*email: paolo.annibale@mdc-berlin.de, pa53@st-andrews.ac.uk

Abstract

Muscarinic acetylcholine receptors are prototypical G protein-coupled receptors (GPCRs), members of a large family of seven transmembrane receptors mediating a wide variety of extracellular signals. We show here, for the first time in a GPCR, that the carboxyl terminal fragment of the muscarinic M_2 receptor, comprising the transmembrane regions 6 and 7 (M_2tail), is expressed by virtue of an internal ribosome entry site located in the third intracellular loop. Single cell imaging reveals that M_2tail, whose expression is upregulated in cells undergoing integrated stress response, does not follow the normal route to the plasma membrane, but is almost exclusively sorted to the mitochondria inner membrane: here it controls oxygen consumption, cell proliferation and the formation of reactive oxygen species by reducing oxidative phosphorylation. Crispr/Cas9 editing of the key methionine where cap-independent translation begins in human induced pluripotent stem cells, reveals the physiological role of this process in influencing cell proliferation and oxygen consumption at the endogenous level. The expression of the C-terminal domain of a GPCR, capable of regulating mitochondrial function, constitutes a hitherto unknown mechanism notably unrelated to its canonical signalling function as a GPCR at the plasma membrane. This work thus highlights a potential novel mechanism thar cells may use for controlling their metabolism under variable environmental conditions, notably as a negative regulator of cell respiration.

Introduction

Muscarinic receptors include five structurally related receptors, belonging to class A of the G protein-coupled receptor (GPCR) family [1]. They are comprised of seven transmembrane domains (TM domains 1-7) connected by intra and extracellular loops. Of these structural elements, the third intracellular (i3) domain is the one conferring a coupling specificity for G proteins, β-arrestin recruitment and endocytic internalization [2]. However, only a small portion of the i3 loop is required for receptor function, and for this reason large deletions of this segment have no effect on receptor activation and internalization [3].

GPCRs are normally distributed at the plasma membrane, where, after activation by an agonist and coupling to either G proteins or β-arrestin, regulate a number of intracellular effectors. Nevertheless, non-canonical localizations of GPCRs have also been described, such as in

endosomes [4], cell division compartments (centrosomes, spindle midzone and midbodies) [5] and mitochondria [6, 7], underpinning non-traditional roles for this protein family.
Several studies have shown that the GPCR structurally related transmembrane protein bacteriorhodopsin consists of autonomous folding domains that translocate to the membrane and interact with each other to function as a proton pump. Interestingly, it was also shown that fragments of muscarinic receptors can interact to form functionally active chimeric receptors, highlighting the conserved evolutionary ability of domains from these receptor family to interact among each other, as well as with other proteins. Intriguingly, in 2016, we observed that the insertion of a stop codon in the third intracellular loop of the muscarinic M_2 receptor was not able to abolish its function [8], presenting the suggestive possibility that a cap-independent translation of the M_2 C-terminal domain may occur in this mutant, i.e. that the M_2 mRNA may lead to the translation not only of the full length receptor, but also of its C-terminal domain, that we name here M_2tail.

In this work, we therefore set out to explore whether the expression of the M_2tail, a region containing the TM regions 6 and 7, occurs naturally by a cap-independent translation mechanism. Combining radio-ligand binding, molecular biology approaches, advanced fluorescence imaging and Crispr/Cas9 genetic editing of human induced pluripotent stem cells (hiPSCs) we have gathered compelling data indicating a novel translation mechanisms for C-terminal domain of the M_2 muscarinic receptor under control of a IRES sequence within the M_2 mRNA and that the C-terminal domain of this receptor can indeed be expressed as an independent polypeptide.

While in eukaryotes the most common mechanism of translation initiation is the cap-dependent process, which requires the interaction of several key proteins at the 5'-end (5′ cap) of mRNA molecules, recent years have seen growing evidence that internal ribosome entry site (IRES) sequences, which are common features of virus replication [9], can mediate cap independent translation of eukaryotic RNA(s) [10].

Moreover, by using bimolecular fluorescence complementation, in-vitro mitochondrial import and cell metabolism assays we observe that M_2tail is strongly targeted to the cell mitochondria. Importantly, this mitochondrial targeting has functional ramifications since both cap-dependent mediated overexpression of M_2tail, as well as cap-independent mediated translation starting from the mRNA of the full length M_2 receptor, resulted in a sizable reduction of oxidative phosphorylation. In fact, we show that cellular stress favours the activation of this newly

92 discovered IRES-dependent translation of M_2tail and that the fragment interacts with the Complex
93 V of the respiratory chain on the mitochondria inner membrane. The implication of this newly
94 discovered regulatory mechanism of the IRES mediated translation of the M_2 C-terminal domain
95 might have profound physiological and pathophysiological implications.
96
97 In summary our study reports the new observation that alternative reading of a GPCR receptor
98 gene can translate into a fragment of the receptor that serves a cellular function entirely different
99 from canonical GPCR signalling**.** Taken together these data strongly suggest that the M_2 mRNA
100 yields not only a plasma membrane receptor able to transduce many of the acetylcholine functions
101 but M_2tail, a protein fragment that reduces the activity of mitochondria and ROS accumulation and
102 it might represent a hitherto unappreciated step for in-vivo anti-oxidative stress, during for instance
103 reperfusion, tissue damage, and disease-promoted metabolic cellular stress.
104
105
106 ## Results

107 **Cap independent production of the C-terminus of the M_2 receptor and evidence for**
108 **an IRES**
109 We began our work by testing our earlier hypothesis that the last two TM regions (TM6-7) of
110 M_2stop228, a M_2 muscarinic receptor mutant bearing a stop codon at the beginning of the i3 loop
111 in position 228 (**Fig. S1**), may still be translated [11]. We thus generated EGFP C-terminal fusion
112 of the M_2 wt receptor and M_2stop228: **Fig. 1A** shows that cells expressing M_2stop228-EGFP
113 display a green fluorescence signal. Moreover, the signal displays a predominant intracellular
114 localization with respect to the wt M_2R, which instead localizes -as expected- largely at the plasma
115 membrane. A key observation is that the position of the stop codon upstream of the i3 loop
116 appears to bear a particular relevance, since if a stop is instead inserted downstream of position
117 228, e.g. at positions 400, right before the first methionine in TM6, no fluorescence can be
118 observed in cells expressing the mutant M_2stop400-EGFP **Fig. 1A.**
119
120 To further appreciate the origin of this unexpected process -the 228 stop codon should abolish
121 any EGFP signal- we performed radioligand binding experiments in cells transfected with this
122 mutant. M_2stop228 showed both K_D value of [^{3}H]NMS (N-methylscopolamine, an antagonist)
123 calculated from direct saturation experiments, and the IC_{50} values, calculated in competition
124 experiments for the agonist carbachol, similar to those calculated for the wild type M_2 receptor

125 (**Table 1**), albeit displaying a very low level of expression at the plasma membrane, i.e. 45 fmol/mg
126 of protein. Furthermore, M_2stop228 was found functionally active as it was capable to inhibit
127 adenylyl cyclase [10] and increase ERK phosphorylation (**Fig. S2A**), even though the extent of
128 response was reduced if compared to the wild type M_2 receptor (**Table 1**). As a control, receptor
129 fragments, translated from mRNAs comprising only the sequence for TM1-5 (i.e. whose
130 sequences run only until position 228 or 283 of the corresponding full length receptor), called
131 M_2trunk(1-228)/M_2trunk(1-283), did not show any radio-ligand binding activity, despite coding for
132 the same first five trans-membrane regions (TM1-5) that the canonical translation of M_2stop228
133 should also produce (**Fig. 1B** and **Table 1**) [12].
134
135 We showed in the past that the last two TMs (TM6-7) of the M_2 receptor can reconstitute a
136 functional receptor with TM1-5 [12] (**Table 1**), supporting the notion that the explanation of the
137 apparent paradox of M_2stop228 must be that M_2tail is translated as an independent polypeptide,
138 as graphically summarized in **Fig. 1B**.

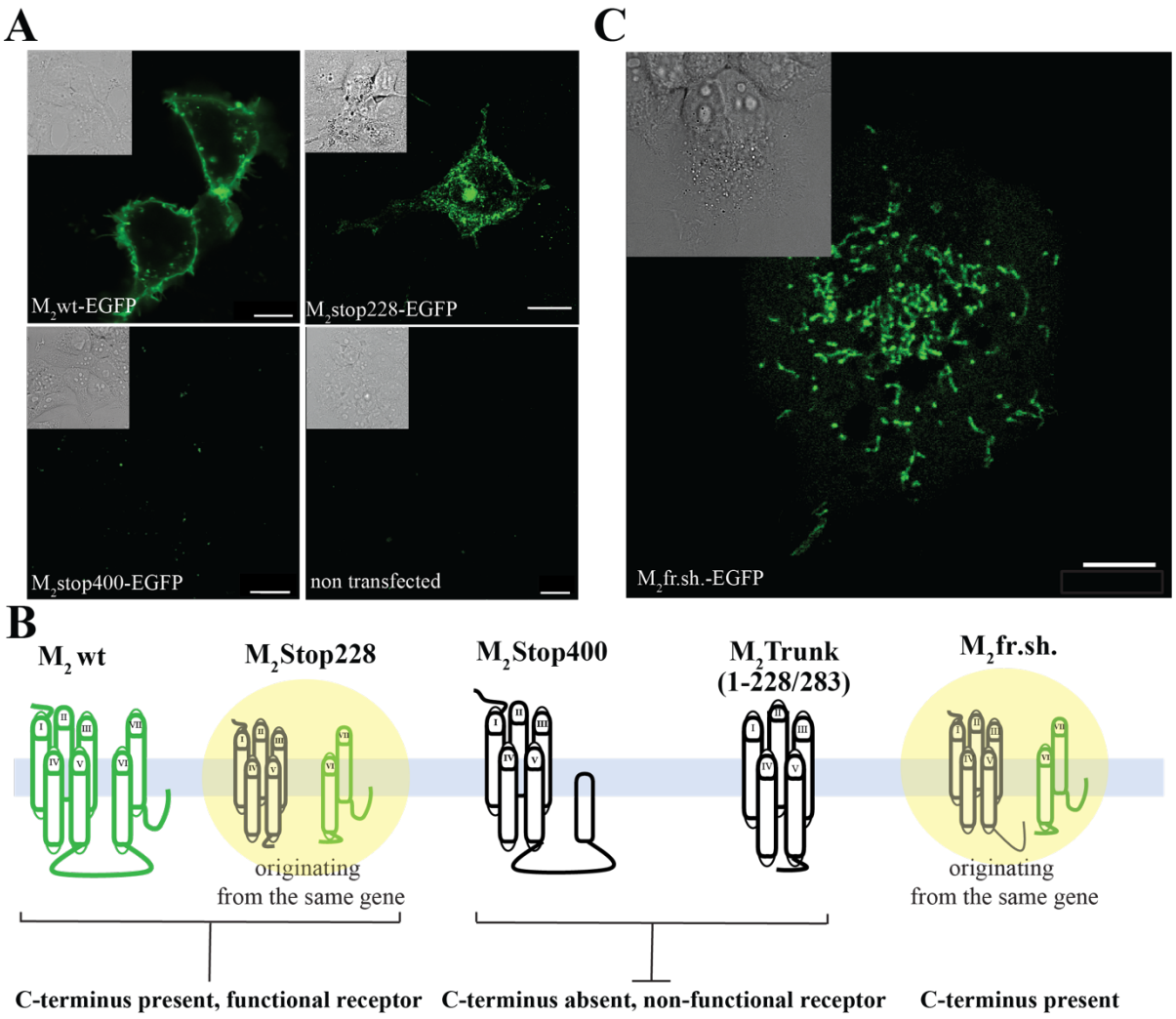

Fig. 1. The c-terminus of the M_2 receptor is expressed by a cap independent translation mechanism, originating in the i3loop.

A, Fluorescence micrographs of HEK293 and COS7 cells respectively expressing M_2-EGFP, M_2stop228-EGFP, M_2stop400-EGFP, together with an untransfected control. **B**, Schematic representation of the gene products that reach the plasma membrane of the wild type M_2, M_2stop228, M_2trunk(1-283) and M_2fr.sh. (**Fig. S3**). **C**, Fluorescence micrograph of a representative HEK293 cell expressing M_2fr.sh.-EGFP. Insets display DIC image of the same field of view (scale bar 10 μm). Imaging settings are the same for the f images, whereas contrast was adjusted to improve visualization. In the untransfected cells and stop400 panels, the contrast was set to 0. Insets display DIC image of the same field of view (scale bars 10 μm).

Binding data				Adenylyl cyclase inhibition assay	
Receptor	Bmax (fmol/mg)	[^{3}H]NMS KD (pM)	Carbachol IC50 (μM)	Carbachol EC50 (μM)	Maximum inhibition of forskolin stimulated cAMP accumulation (%)
M_2	980 ± 60	62 ± 7	2.1 ± 0.6	0.04 ± 0.01	53 ± 5
M_2trunk(1-283)	N.B.				
M_2trunk(1-228)	N.B.				
M_2stop228	45 ± 2	70 ± 10	1.8 ± 0.4	0.13 ± 0.02	27 ± 3
M2trunk(1-283) +M2tail(M-281-466)	480 ± 20	79 ± 10	0.7 ± 0.2	0.15 ± 0.03	37 ± 4
M2trunk(1-228) +M2tail(368-466)	70 ± 10	72 ± 8	0.6 ± 0.2	0.17 ± 0.03	29 ± 4

Table 1. Radioligand binding and activation properties of M_2 receptor mutants.

Binding properties and inhibition of forskolin stimulated adenylyl cyclase by M_2, M_2stop228, M_2trunk(1-228), M_2trunk(1-283), and cotransfected M2trunk(1-283) + M2tail(M-281-466) and. M2trunk(1-228) + M2tail(368-466). Untransfected COS-7 cells did not show any [^{3}H]NMS specific binding. N.B. = no specific [^{3}H]NMS binding. Data are averages with s.e.m.

Evidence of an IRES-mediated M_2 C-terminus translation

M_2stop228 mRNA appears thus able to give rise -despite the presence of a stop codon in the i3 loop- to two distinct protein products (a *trunk* TM1-5 and a *tail* TM6-7), in turn able to reconstitute a functional receptor at the plasma level.

To challenge this hypothesis and gain further insight into the mechanism at play, we generated a frame shift mutant of the M_2 receptor: we inserted a single guanine nucleotide in the sequence of the M_2-EGFP, changing the methionine in position 368 into an aspartate, which in turn generates an in-frame stop codon at position 370 (**Fig. S1 and Fig. S3**). The observation that cells transfected with M_2fr.sh.-EGFP retain green fluorescence is most remarkable (**Fig. 1C**), since the

167 EGFP is now out of the original reading frame and it can only be properly translated by a *cap-*
168 *independent translation mechanism*, starting from a methionine in the new reading frame.
169 Furthermore, the observation that both M_2stop228-EGFP and M_2fr.sh.-EGFP retain green
170 fluorescence, whereas M_2stop400-EGFP does not, indicates not only that a cap independent
171 translation mechanism occurs, but also that the starting methionine for the process must be
172 downstream of stop 228 and upstream of stop 400, leaving as a leading candidate one of the in-
173 frame methionines of the i3 loop.
174 To narrow this down, we employed radio-ligand binding data from expression of receptor mutants
175 carrying a double stop codon, the first in position 228 and the second in positions ranging from
176 248 to 400, including mutations of the first (M248) and second (M296) in-frame methionines in the
177 third i3 loop (**Table S1**, **Fig. S3**). The observation that mutation of the first two methionines does
178 not affect B_{max} points to M368 as the most likely site for the cap-independent initiation of translation
179 of the M_2tail, that we now term more specifically M_2tail(368-466). These binding results can
180 furthermore rule out read-through and termination re-initiation: if these mechanisms were
181 responsible for translation of the C-terminal of the M_2stop228, suppression of the first methionine
182 would have abolished the binding. We shall further note that cells expressing M_2stop228 showed
183 only one single M_2 specific cDNA band supporting the concept that the M_2tail(368-466) was
184 produced from the same M_2-mRNA molecule by a cap independent mechanism instead of, for
185 instance, by RNA splicing variants (**Supplementary Materials and Methods** and **Fig. S2B**).
186

187 **IRES position within the M_2 coding sequence**

188 To further validate the results obtained working with full length M_2 receptor mutants and screen
189 for what nucleotides are important for the IRES activity, we additionally prepared a fluorescence
190 reporter construct in which the i3 loop of M_2 was inserted between the two fluorescent proteins
191 Sirius and EGFP (**Fig. 2A**). The sequence for Sirius is followed by a stop codon, thus making
192 Sirius-M_2i3(417n)-EGFP translate Sirius according to the classical cap-dependent mechanism,
193 reporting on transfection efficiency, and, at the same time, drive EGFP translation only if the M_2i3
194 loop contains an IRES sequence, effectively acting as a bicistronic expression cassette. We
195 transfected several cell lines with this construct, all positive for the blue and green fluorescence
196 (**Fig. S4A**). HEK293 cells, used throughout our study, appeared positive for both the blue and
197 green fluorescence, as shown in the inset of **Fig. 2A** and in line with the results reported in **Fig.**
198 **1A**. To further rule out the possibility that EGFP translation from the Sirius-M_2i3(417n)-EGFP
199 construct could be due to read-through and termination-re-initiation mechanisms, a mRNA hairpin

loop was inserted in the sequence after the stop codon of the Sirius protein (Sirius-H-EGFP), abolishing completely EGFP signal.

To narrow down the position of the IRES sequence we divided the M_2 i3 loop in three parts and the resulting nucleotide sequences, 685-699, 685-1071 and 685-699/1072-1101, were inserted downstream of the hairpin loop in three different constructs (**Fig. 2A** and **Fig. S3**).

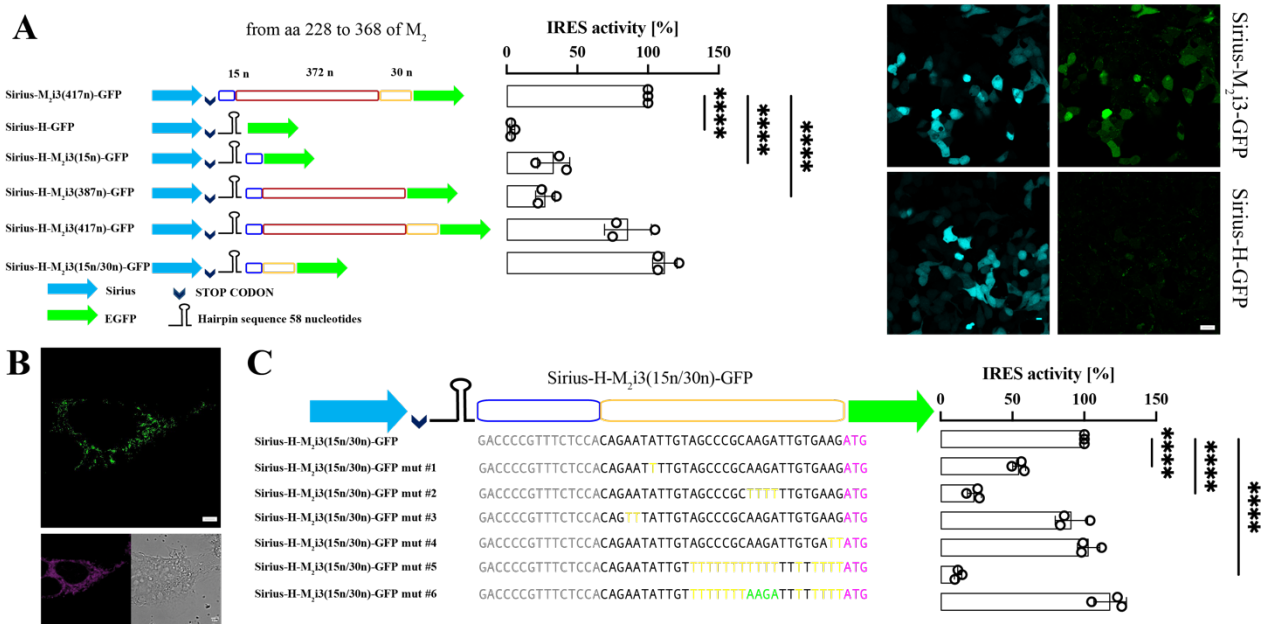

Fig. 2. Localization of the IRES within the i3 loop the muscarinic M_2 receptor using a fluorescence reporter assay.

A, **left** Schematic representation of bicistronic plasmids bearing the M_2 i3 loop between the coding regions of the Sirius and EGFP fluorescent proteins. A guanine nucleotide was originally inserted before the EGFP in the plasmid Sirius-H-EGFP in order to maintain in frame the sequences of the two fluorescent proteins. In all the other plasmids the sequence of the two fluorescent proteins is not in frame. Fifteen nucleotides derived from the M_2 i3 loop were inserted between the end of Sirius and the hairpin loop, in order to allow the easy scanning of the ribosome across the stop codon. **right**, IRES activity, highlighting the efficiency of cap-independent translation for the control Sirius-M_2i3(417n)-EGFP and the six mutants. The insert shows the difference in the green fluorescence between two of the mutants. Significance values reported in the graphs were determined by a one-tailed Student t-test, p-values: ** $0.001<p<0.01$. **B,** Expression of the construct M_2-Hairpin-EGFP in HEK293 cells: (top) Confocal images of M_2-Hairpin-EGFP, Mitotracker Deep red staining and DIC (bottom). Scale bar 5 μm. **C**, **left** Mutations of the bicistronic Sirius-H-M_2i3(15n/30n)-EGFP plasmids in the region of the M_2 i3 loop from nucleotides 1972 to 2001, in yellow are the modified nucleotides. In Sirius-H-M_2i3(15n/30n)mut#6-EGFP the four nucleotides in green (AAGA) were reinserted

222 in the stretch of 20 T of Sirius-H-M_2i3(15n/30n)mut#5-EGFP. **right** IRES activity, highlighting the efficiency
223 of cap-independent translation for the control Sirius-H-M_2i3(15n/30n)-EGFP and the six mutants illustrated.
224 Significance ($p < 0.01$) was calculated in **A** against Sirius-M_2i3(417n)-EGFP and in **B** against Sirius-H-
225 M_2i3(15n/30n)-EGFP. Error bars are s.e.m. Significance values reported in the graphs were determined by
226 a one-tailed Student t-test, p-values: ** $0.001<p<0.01$.
227
228 When the full i3loop was placed after the hairpin, green fluorescence was fully recovered and the
229 resulting construct (Sirius-H-M_2i3(417n)-EGFP) showed only a slight reduction of the EGFP/Sirius
230 with respect to the value measured for the analogous reporter without hairpin (~90%) (**Fig. 2A**).
231 Finally, when the last portion of the M_2 i3 loop was inserted in the construct after the Hairpin,
232 leading to Sirius-H-M_2i3(15n/30n)-EGFP, ~110 % of the value measured for the Sirius-M_2i3(417n)-
233 EGFP plasmid was recovered (**Fig. 2A**). Notably, when the hairpin was inserted within the i3 loop
234 of the full length M_2-EGFP, upstream of the M368, it was still possible to observe green
235 fluorescence in transfected cells (**Fig. 2B**).
236
237 These results confirm that the IRES is located in a region of the i3 loop sequence immediately
238 upstream of the third methionine (M368). This is also confirmed from ribosome profiling data from
239 human left ventricle tissue, displaying increased p-sites as well as overall ribosomal coverage in
240 correspondence of this region (**Fig. S4B**). Based on this evidence, we mutated the conserved
241 residues highlighted in yellow in **Fig. S4C,** in order to check for their relevance in recruiting the
242 ribosome on the M_2 i3 loop sequence, as shown in **Fig. 2C**. As discussed in detail in the
243 **Supplementary Materials**, we found that the four nucleotides AAGA1090-1093 next to the
244 methionine 368 play a pivotal role in recruiting the ribosome on the M_2 mRNA and in translating
245 the M_2 C-terminal fragment.
246
247 **Generalization to other members of the GPCR superfamily**
248 In order to determine if the observed behavior is specific to the M_2 receptor or could highlight a
249 feature common to other members of the GPCR superfamily, we repeated several of our
250 experiments in another GPCR, the related muscarinic M_3 receptor. The M_3 displays an in-frame
251 methionine at the end of the i3loop, in position 481. We then inserted a stop codon in position
252 273, generating the construct M_3stop273 that still displayed radio-ligand binding and functional
253 activity (**Table S2**). Several other mutants, mimicking the single and double stop mutations
254 performed for the M_2 displayed a behavior consistent with M481 being the start point of a cap-
255 independent translation of the C-terminal also for the M_3 receptor (**Table S2**), thus indicating that

256 IRES-mediated cap-independent translation of the C-terminal domain could be a phenomenon
257 not restricted solely to the M_2 receptor, but may be shared at least by some other members of the
258 GPCR superfamily. The presence of an IRES sequence upstream of M481 further appears to be
259 supported by the observation of GFP fluorescence when 558 nucleotides from the i3 loop of the
260 M_3 receptor (from nucleotide 880 to 1437) were inserted in the same Sirius-EGFP reporter
261 construct as used for the M_2 (**Fig. S5B**). This appears to be indeed supported by the sequence-
262 alignment of the five muscarinic receptors. The alignment of the last portion of the M_2 i3 loop (from
263 nucleotide 1072 to 1104) with regions adjacent to the second (M_1), fourth (M_3 and M_4) and first
264 (M_5) in-frame Methionines, clearly shows that some nucleotide residues are conserved (**Fig. S4C**).
265 Overall these data underline that cap-independent translation could be a more general feature of
266 GPCRs mRNAs.
267

268 **Mitochondrial localization of the M_2 C-terminal fragment generated by cap-dependent**
269 **expression under the control of a viral promoter**

270 After having established that the expression of the M_2 C-terminal domain is regulated by an IRES
271 and that its translation starts with M368, we went on to study the role it might play in the cell. For
272 this purpose, we fused M_2tail(368-466) to EGFP in pcDNA3, that is under the control of a strong
273 CMV promoter, and we expressed it in HEK293 cells in order to study its subcellular localization.
274 Confocal microscopy demonstrated a striking mitochondrial localization of the M_2tail(368-466)-
275 EGFP construct (**Fig. 3A**).
276 We confirmed this observation by co-staining HEK293 cells with a conventional mitochondrial
277 stain and by co-expressing M_2tail(368-466)-EGFP with Tom20-mCherry, a marker for the outer
278 mitochondrial membrane (**Fig. S6A**). The observed mitochondrial localization of M_2tail(368-466)-
279 EGFP appeared in stark contrast to the canonical cellular localization of the M_2 receptor, as shown
280 in **Fig. 3b** where the M_2 muscarinic receptor was C-terminally labeled with the red fluorescent
281 protein mRuby2. In line with the radioligand binding data shown in **Table 1**, very little expression
282 of M_2tail(368-466)-EGFP was observed on the plasma membrane, as we confirmed by
283 fluorescence correlation spectroscopy (FCS) [13] (**Figs S6B-D**). By contrast, when the M_2tail(368-
284 466)-EGFP was co-expressed with M_2stop228, an increased localization could be seen on the
285 cell membrane, suggesting a chaperon activity of the M_2 N-terminal domain (M_2trunk) (**Figs S6E-**
286 **G**). Likewise, constructs such as M_2tail(368-466)-mRuby2 (a red monomeric fluorescent protein)
287 and M_2tail(368-466)-tdTomato (a tandem-dimer red fluorescent protein) also displayed clear
288 mitochondrial localization (**Figs S6H-I**), ruling out bias due to the fluorophore used. We obtained
289 comparable findings also in COS-7 cells (**Fig. S6J**).

Mitochondrial import of the C-terminal fragment of the M_2 receptor was further verified by immunoblotting of protein extracts from purified mitochondria of HEK293 cells transfected with myc-tagged M_2 receptor, M_2tail(368-466) and M_2M368A, a mutant where the key methionine for the cap-independent translation of the C-terminus is changed to an Alanine. **Fig. 3C** shows that in purified mitochondria (unlike in the cytosolic and microsomal supernatants originating from the purification process, **Fig. S6K**), only the protein bands associated to the M_2 C-terminal fragment were visible. Notably, no mitochondrial import was visible for the M_2M368A, confirming that the third in-frame methionine (M368) in the i3 loop of the M_2 receptor is necessary for the C-terminal fragment production and its localization to the mitochondria. The slight offset between the lower bands in the M_2 wt and M_2tail(368-466) lanes matches exactly the different length of the linker used to fuse the myc-tag in the two constructs.

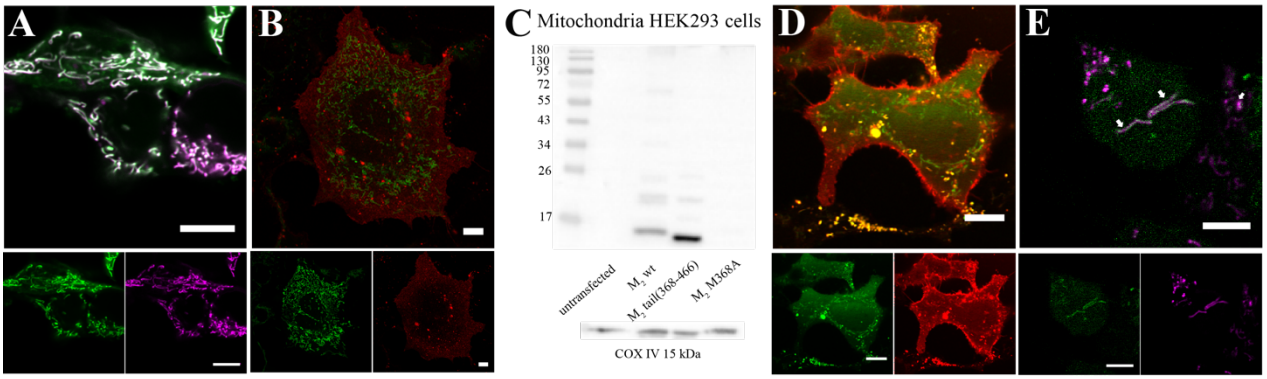

Fig. 3. M_2tail(368-466) predominantly localizes to the cell mitochondria

A, Colocalization of M_2tail(368-466)-EGFP (green) together with the mitochondrial targeted dye Mitotracker (magenta) in HEK293 cells. Separate spectral channels are displayed below. **B**, Co-expression of M_2tail(368-466)-EGFP (green) and wild type M_2-mRuby2 (red) in HEK293 cells. Separate spectral channels are displayed below. **C**, Western blot (10% TRIS-Glycine PAA gel) of mitochondria purified from Hek293 cells transfected with the M_2-myc, M_2tail(368-466)-myc, M_2M368A-myc, together with an untransfected control are blotted using an anti-myc antibody. Loading control was verified by immunoblotting COXIV. **D**, Cellular localization of the construct M_2-mRuby2-STOP-M_2-i3-tail-EGFP in HEK293 cells. Expression of the M_2tail(368-466)-EGFP (green) after the STOP codon is an indicator of the endogenous IRES activity. While M_2-mRuby2 localizes correctly and predominantly to the cell plasma membrane, M_2tail(368-466)-EGFP localizes intracellularly. Separate spectral channels are displayed below. **E**, M_2-fr.sh.-EGFP (green) expressed in conjunction with Mitotracker (magenta). The EGFP is expressed despite the creation of an in-frame stop after M368, confirming endogenous cap-independent translation of the M_2tail(368-466). Arrows indicate areas of colocalization with the mitochondria. Separate spectral channels are displayed below.

317 **Localization of the M_2 C-terminal fragment generated by cap-independent expression**
318 **under the control of the i3loop IRES**
319 We then sought to express the M_2tail under the control of the i3loop IRES rather than a viral
320 promoter, to further exclude the possibility that the observed mitochondrial localization of the M_2
321 carboxyl terminal fragment were due to overexpression of the construct. HEK293 cells were
322 transfected with the construct M_2-mRuby2-STOP-M_2-i3-tail-EGFP which contains the full wildtype
323 M_2 receptor, labeled at the C-terminal with mRuby2, additionally fused to the C-terminal part of
324 the M_2 receptor starting at nucleotide 685 of the i3 loop, following the stop codon of mRuby2, and
325 ending with a C-terminal EGFP sequence (**Fig. S3**). Through this experimental strategy, the
326 expression of M_2tail(368-466)-EGFP is regulated by the IRES, and C-terminal fragment
327 production is therefore close to physiological expression. The expression of EGFP confirmed that
328 the *in vivo* production of the M_2tail(368-466) is regulated by the IRES within the i3 loop. In addition,
329 the processed receptor fragment was eventually observed to be predominantly confined to the
330 cytosol and the mitochondrial network (**Fig. 3D**).
331 Notably, when the M_2-EGFP fusion protein was expressed and the cells were co-stained with
332 Mitotracker, a faint EGFP signal was also observed in the mitochondrial regions (**Fig. S7A**),
333 although the expression of the full-length receptor masks this effect and makes quantification
334 difficult. On the other hand, **Fig. 3E** shows that, when the M_2fr.sh-EGFP mutant was expressed
335 in HEK293 cells, the IRES-generated C-terminal fragment of the M_2 receptor localized to the
336 mitochondria. As mentioned above, in this construct the masking effect of the EGFP fused to the
337 full-length receptor is removed (see also **Fig. S3**). Similar mitochondrial localization was also
338 observed when we transfected HEK293 cells with M_2fr.sh-mRuby2 (**Fig. S7B**), ruling out possible
339 effects due to the specific fluorophore used as a tag. Similar localization patterns were observed
340 when the constructs were expressed in a different cell type, such as the H9c2 rat cardiomyoblast
341 cell lines (**Fig. S7C**).
342
343 **Mechanism M_2tail import into the mitochondria and localization within the organelle**
344 To gain further insight into the dynamics and mechanisms of the M_2 C-terminal fragment import
345 within the mitochondria, we first monitored the kinetics of colocalization between mitochondria
346 and EGFP in cells transfected with M_2tail(368-466)-EGFP. In cells observed for several hours,
347 starting at 5h after transfection (**Fig. 4A**), the construct was found initially expressed in the
348 perinuclear region, likely the endoplasmic reticulum, indicating that at least the initial step of
349 subcellular trafficking of the M_2tail(368-466)-EGFP is the same as for the full length receptor [14].
350 At this time (5h post-transfection), almost no colocalization with the Mitotracker-stained

351 mitochondria was visible. However, at 6h post-transfection, the colocalization level increased
352 significantly, and M_2tail(368-466)-EGFP was either found in the cytosol or in the mitochondria. At
353 9h post-transfection the colocalization at the mitochondria was well visible (see **Materials and**
354 **Methods**) and we could observe that almost half of the mitochondrial import occurred within 6h
355 post-transfection (**Fig. 4B**).
356 This value is qualitatively in agreement with what we observed using an in-vitro assay to determine
357 the import of the M_2 carboxyl terminal into isolated mitochondria (see **Materials and Methods**).
358 To this end, we used mitochondria form *S. cerevisiae*, which is a robust and well-studied system
359 for protein import assays. **Fig. 4C** shows the autoradiography experiment of isolated, intact,
360 mitochondria incubated with 35S-labelled full length muscarinic M_2 receptor or M_2tail(368-466),
361 made using a reticulocyte in vitro translation system. The data show that the full-length receptor
362 was not imported into mitochondria. On the other hand, the M_2tail(368-466) displays a clear
363 mitochondrial import already after 5 minutes and increasing over time, up to 30 minutes.
364 Interestingly, this import appears to be independent upon the transporters of the outer membrane
365 Tom5, Tom6, Tom7 and Tom70 (**Fig. S7D**), whereas the import of an inner membrane protein,
366 the ADP/ATP carrier (AAC), used here as a control, depends on Tom70. Upon extraction with
367 carbonate most of M_2tail(368-466) was found in the pellet, and therefore presumably integrated
368 in mitochondrial membranes. Furthermore *Blue native* analysis suggests that the mitochondrially
369 imported M_2tail(368-466) is not a monomer but rather it is part of a larger complex of approximately
370 180 kDa (**Fig. S7D**).
371 All together these data indicate that the import of the M_2tail(368-466) leads to its localization in
372 one of the mitochondrial membranes, to form a complex with other native mitochondrial proteins.
373
374 To further discriminate if the construct is on the outer or inner mitochondrial membrane, we set
375 up a fluorescence assay based upon GFP fluorescence complementation [15] . HEK293 cells
376 were first transfected with two constructs: M_2tail(368-466)-GFP11, in which a short 16 amino acids
377 peptide of GFP was fused at the C-terminus of M_2tail(368-466), and mito-GFP1-10, in which the
378 COX8A was N-terminally fused to the other GFP fragment containing the remaining 10 beta
379 strands (See **Materials and Methods**). **Figure S8A** shows the successful recombination of the
380 two within the mitochondrial matrix. This observation is supported by a set of controls that include
381 a mitochondrial intermembrane space-targeted protein achieved using the targeting sequence of
382 SMAC [16]:(**Figure S8B-D** show a set of positive recombination controls using respectively
383 SMAC-GFP11+SMAC-GFP1-10, mito-GFP11+mito-GFP1-10 and M_2tail(368-466)-GFP11+
384 M_2tail(368-466)-GFP1-10, all displaying mitochondrial recombination comparable to what is

385 ovbserved in Figure S8A for M_2tail(368-466)-GFP11+mito-GFP1-10. As negative controls we
386 observed the lack of complementation of M_2tail-GFP11 with SMAC-GFP1-10 (**Figure S8E**), and
387 the absence of any significant signal when mito1-10 was expressed alone (**Figure S8F**). We then
388 applied this approach to the full length M_2 receptor, by generating the M_2-GFP11 construct and by
389 transfecting it in HEK293 cells. **Fig. 4D** shows a green signal from the recombined GFP visible in
390 the mitochondria. All together these data suggest that the M_2 C-terminal fragment is localized in
391 the inner mitochondrial membrane, with its own C-terminal domain facing the matrix..This
392 interpretation is also finally confirmed by Immuno Electron Microscopy (IEM) imaging of thin
393 sections from cells expressing the M_2stop228 C-terminally labeled using a myc-tag after immune-
394 gold labelling (**Fig. 4E**). As shown in **Figs 4F-G**, gold particles were observed only in mitochondria,
395 and at this stage they appeared localized either to the mitochondrial matrix or to the lumen of the
396 cristae (**Figs 4H-K**).
397
398 **Cell stress upregulates IRES-mediated M_2tail expression and drives mitochondrial**
399 **localization**
400 Having established that M_2tail localizes in the inner mitochondrial membrane we then moved to
401 look at the effect of stress on the level of expression of the C-terminal fragment. Stressed cells
402 are known to attenuate their translational activity via phosphorylation of the initiation factor eIF2α.
403 However, certain mRNAs may be insensitive to eIF2α phosphorylation level if their translation is
404 regulated by IRES, and under these conditions their expression is bound to increase rather than
405 to attenuate [17, 18].
406 Therefore, we transfected COS-7 cells with the Sirius-M_2i3(417n)-EGFP reporter construct and
407 stressed by starvation for three hours by replacing the culture medium with HBSS or phosphate
408 saline buffer (PBS). Notably, PBS has a poorer nutrient content than the HBSS media, thus
409 causing a more pronounced starvation. During this time interval, the green fluorescence was seen
410 to gradually increase up to 1.4 times the basal level observed in HBSS-starved cells and 3.5 times
411 for PBS-starved cells (**Fig. 5A**), confirming that the C-terminal fragment expression is upregulated
412 in response to stress conditions such as cell starvation. The same experiment was reproduced in
413 single cells, displaying an increase of the average EGFP/Sirius ratio (slope), and thus of IRES-
414 mediated translation, upon HBSS starvation in HEK293 cells (**Fig. 5B**). We further used the GFP
415 fluorescence complementation assay to emphasize the importance of stress in the pattern of
416 expression of the M_2 gene. HEK293 cells were co-transfected with M_2-GFP11 and Mito-GFP1-10.
417 HEK293 cells grown in culture medium predominantly expressed the full M_2 receptor protein (**Fig.**
418 **5C**).

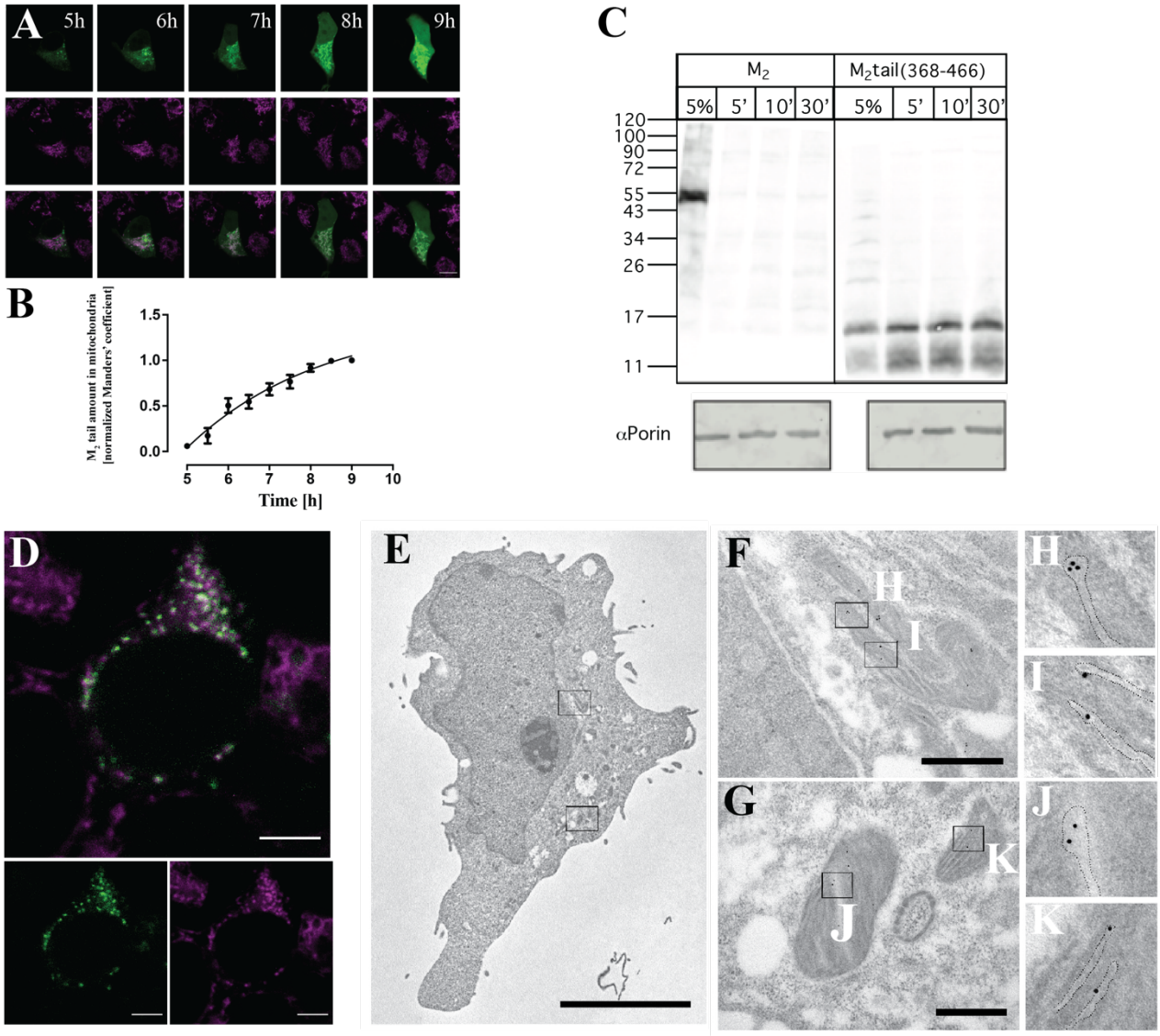

Fig. 4. Mitochondrial import and organelle localization of M_2tail

A, Time course of M_2tail(368-466)-EGFP import in the mitochondria of a HEK293 cell over a 4h interval, starting 5h after cell transfection, as indicated. Panels, from top to bottom show M_2tail(368-466)-EGFP (green), Mitotracker (magenta) and overlay displaying increasing colocalization over time. **B**, Quantification of the colocalization of the M_2tail(368-466)-EGFP in the mitochondria by calculating the Manders Coefficients (n=7 cells, from 3 independent transfections, error bars are s.e.m.). **C**, Import of protein M_2tail(368-466) in isolated yeast mitochondria: ^{35}S-labelled and translated in-vitro full length muscarinic M_2 receptor or M_2tail(368-466) expressing 5 C-terminal Methionines were with isolated yeast mitochondria for 5, 10 and 30 minutes in the presence of the inner membrane potential The 5% lane represents a control with the pure protein, with no mitochondria. αPorin is used as a loading control.. **D,** Detail of a HEK293 cell expressing the M_2-GFP11 construct together with mito-GFP1-10. The M_2-GFP11 was sequentially

transfected 24 h after the mito-GFP1-10 Magenta indicates mitotracker. White signal in the overlay indicates M_2tail(368-466) trafficking to the organelle. All confocal micrographs were obtained by sequential imaging using 488 nm excitation and detection in the 520-600 nm (EGFP), and at 633 nm and detected in the 650-700 nm range (Mitotracker) using HyD detectors in Photon Counting Mode. Scale bars are 10 µm throughout. **E,** Representative Immuno Electron Microscopy (IEM) micrograph of a COS-7 cell showing a large nucleus, several mitochondria and vacuoles nearby. Bar: 5 µm. **F-G**, High magnification of portion of the cell cytoplasm showing a few gold particles confined to the mitochondria. Bar: 500 nm. **H-K,** Gold particles appear associated with the mitochondrial cristae, highlighted by the dotted line. A total number of 236 gold particles in 40 mitochondria from 19 sections were detected.

The green fluorescence detected at the plasma membrane is explained with the chaperoning effect of M_2-GFP11 on Mito-GFP1-10 before its sorting to the mitochondria. In sharp contrast, when HEK293 cells were first transfected with Mito-GFP1-10 and, 24h later, transfected with M_2-GFP11 followed by a 6 h starvation in HBSS, the pattern of expression changed drastically: IRES mediated translation of the M_2tail(368-466) fragment led to a predominantly mitochondrial green fluorescence signal of the complemented GFP (**Fig. 5D**). These results are in line with our observation that the IRES mediated C-terminal fragment localization to the mitochondria in cells expressing the construct M_2-mRuby2-STOP-M_2-i3-tail-EGFP was enhanced upon cell starvation, and drastically reduced upon mutation of the M368 (**Figure S9** and **Supplementary Materials**).

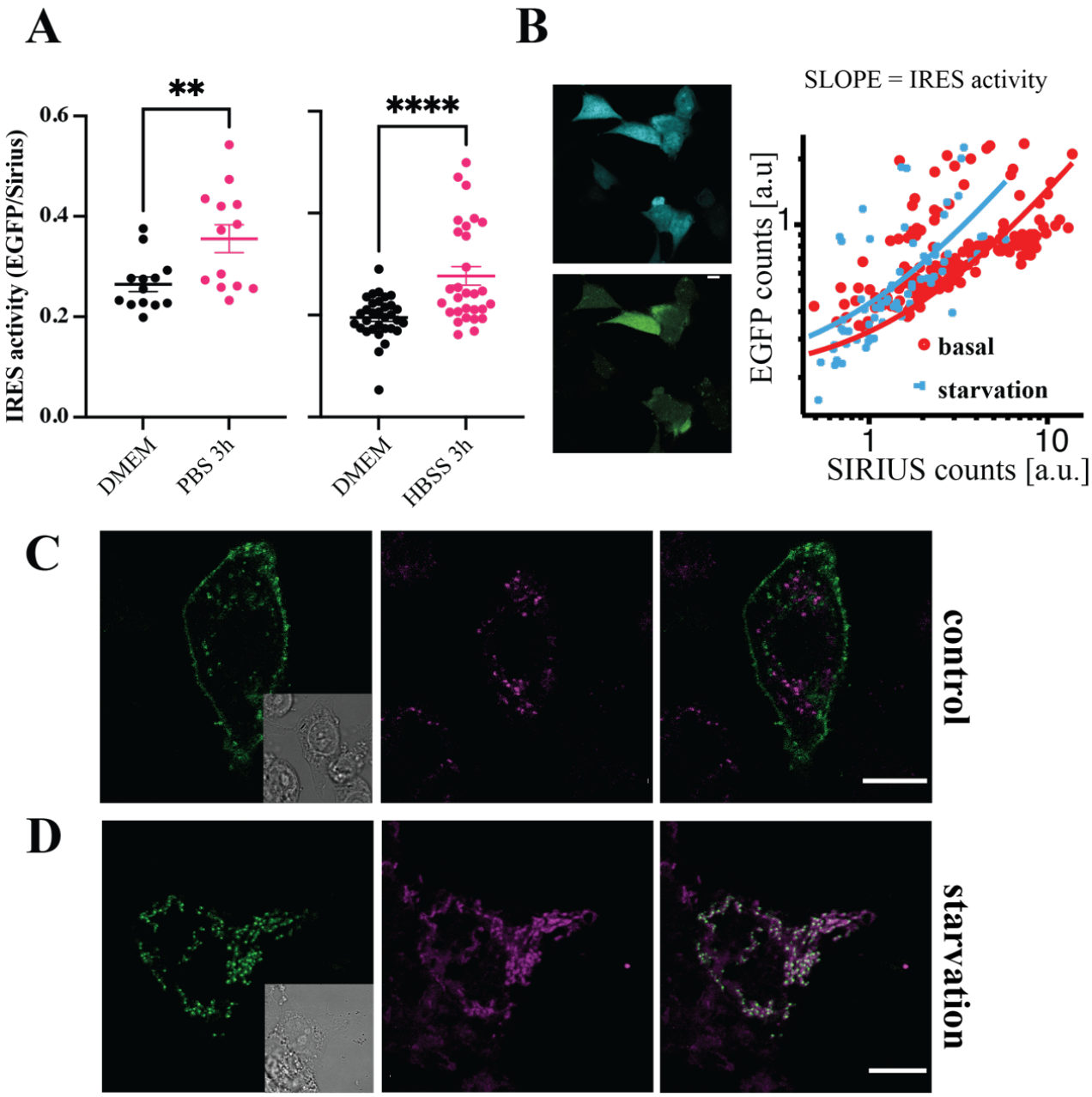

Fig. 5 Effect of integrated stress response on IRES activity and M_2tail(368-466) localization

A, 96-well plate reader measurement of the increase of EGFP fluorescence relative to Sirius in COS-7 cells transfected with the bicistronic Sirius-M_2i3(417n)-EGFP plasmid and starved for three hours respectively in PBS (left panel) (n= 3 transfections, 16 wells) and HBSS (right panel) (n=1 transfection, 16 wells). Significance values reported in the graphs were determined by a one-tailed Student t-test, p-values: **** $p<0.0001$; ** $0.001<p<0.01$. **B,** Single cell measurement of EGFP vs SIRIUS expression in HEK293 cells, in basal conditions and upon starvation. Lines are linear fits (note log-log scale). **C**, HEK293 cells were sequentially transfected with pMito-GFP1-10 (24h) and M_2-GFP11 (8h, of which 6h under starvation

460 conditions) and then grown in full culture medium or **D,** starved for 6 h after transfection of M_2-GFP11.Shown
461 are EGFP fluorescence (left, with DIC inset), Mitotracker (center) and overlay (right). Scale bars are 10 μm.
462

463 **Functional role of the C-terminal fragment in the mitochondria**

464 The next step of our investigation concerned the obvious question about the functional effects that
465 the observed localization of the M_2 C-terminal fragment might have on the mitochondrial activity,
466 and -more generally- on the energy metabolism of the cell. To investigate this aspect, we
467 measured the extent of oxygen consumption in COS-7 cells expressing M_2-EGFP, M_2tail(368-
468 466)-EGFP or the sole EGFP as a control. Initially, we normalized the expression of the three
469 proteins to the amount of EGFP expressed in the cells, then the metabolic functions were assayed
470 on a *Seahorse* instrument using cells transfected with normalized amounts of plasmids (**Fig. 6A**).
471 Our data did not show a significant difference in total oxygen consumption capacity between cells
472 transfected with cytosolic EGFP and the untransfected control. However, a significant decrease
473 of oxygen consumption was found in cells transfected with M_2-EGFP and even more so with
474 M_2tail(368-466)-EGFP (**Fig. 6A**). Notably, the basal oxygen consumption rate (OCR) in starvation-
475 induced stress conditions was profoundly decreased in M_2tail(368-466) cells. This occurred to a
476 smaller extent also in M_2 cells compared to EGFP-transfected and empty control cells (see also
477 the time-course in **Fig. S10A)**. These results are in line with what was observed using a Clarke-
478 type oxygen electrode (**Supplementary Materials and Fig S10B-C**).
479 Notably, there was no difference in the number of apoptotic cells among the different cell groups
480 as shown by the caspase-3 activation assays of apoptosis [19](**Fig. S10D**) and morphological
481 investigation of the mitochondrial network (**Fig. S10E**). To test whether the M_2tail effects on
482 mitochondrial oxygen consumption could alter the production of Reactive Oxygen Species (ROS),
483 the measurements were combined in a single cell assay. Remarkably, ROS production (assayed
484 using a fluorescence readout kit, where the fluorochrome becomes activated in contact with
485 oxidized species) was clearly reduced within and in proximity of mitochondria of cells expressing
486 a high level of the M_2tail(368-466) (**Fig. 6Binset**). By regrouping individual mitochondria in classes
487 according to the level of the ROS marker expression, an inverse correlation between the amount
488 of receptor fragment (Green Fluorescence) and the production of ROS (Red Fluorescence) was
489 revealed (**Fig. 6B)**.
490 Cell growth was also found to be affected depending on which of the constructs was transfected.
491 Notably, transfection of HEK293 cells with full length M_2 receptor reduced significantly cell growth
492 compared to the control, whereas cells transfected with the mutant M_2M368A, that do not express
493 the M_2 C-terminal fragment (**Fig. 6C**), displayed a significantly higher growth. All cells were

incubated with saturating concentration of the M_2 antagonist atropine throughout, in order to exclude effects on cell growth and proliferation due to the canonical receptor signaling.

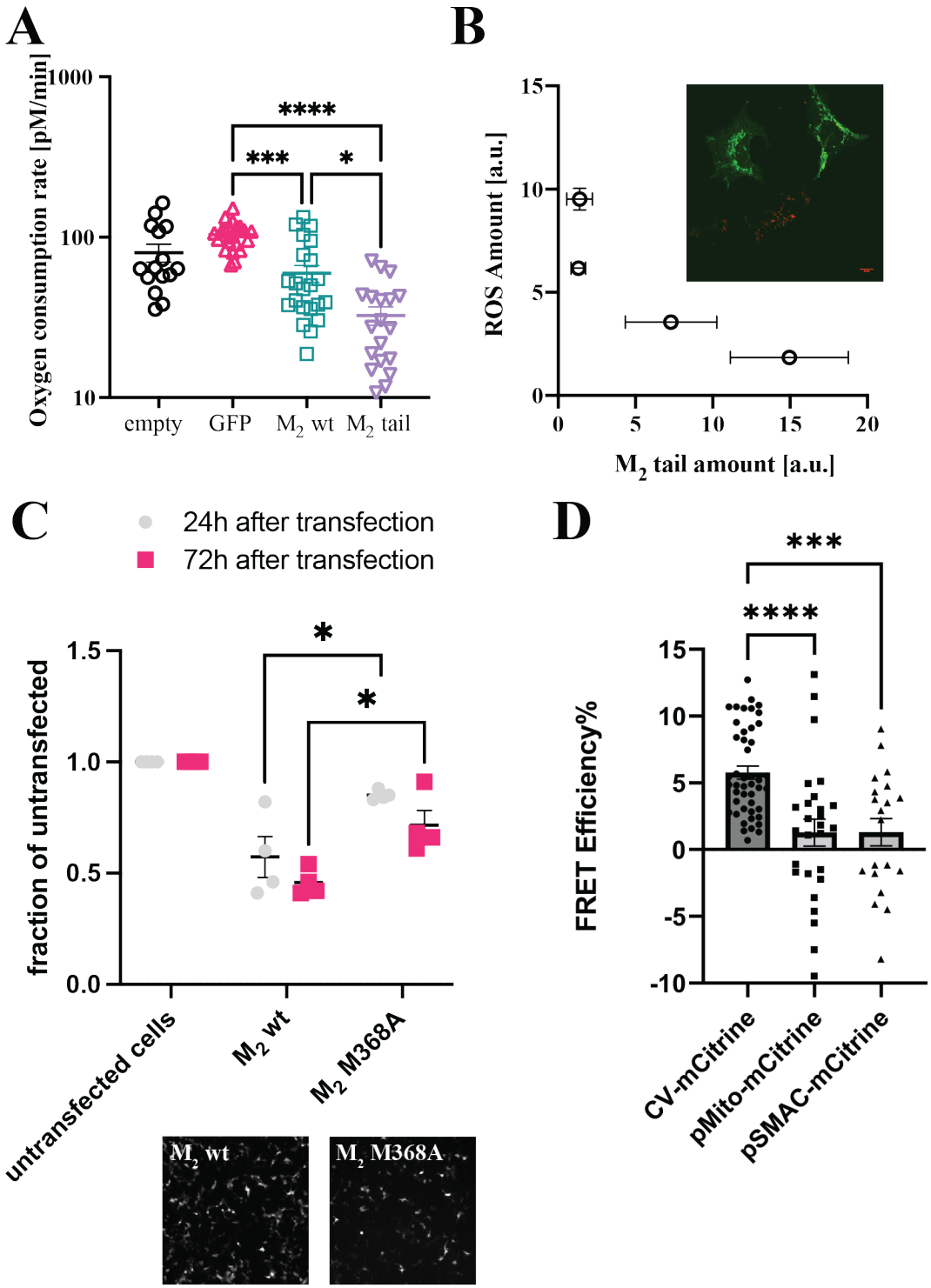

498 **Fig. 6. Effects of M_2tail expression, or absence thereof, on mitochondrial function and cell**
499 **metabolism in transfected HEK293 cells.**

500 **A**, Basal oxygen consumption upon HEK293 cell stress -following starvation- measured by a Seahorse
501 assay at a constant temperature of 37 °C. Significance values reported in the graphs were determined by
502 a one-tailed Student t-test, p-values: **** $p<0.0001$; *** $0.0001<p<0.001$;* $0.01<p<0.05$. **B**, Localization of
503 M_2tail(368-466)-EGFP in HEK293 (green) cells stained with a marker for reactive oxygen species (Cell Rox
504 Deep Red). Relationship between green (M_2tail abundance) vs red (amount of ROS produced) fluorescence
505 intensities measured from regions of the mitochondrial network. The data were binned in four groups as a
506 function of the amplitude of Cell Rox Deep Red signal (0-2.5, 2.5-5. 5-7.5 and 7.5-10 intensity counts). **C**,
507 Cell viability assay performed on HEK293 cells transfected with M_2 and M_2M368A, compared to an
508 untransfected control. Cells were counted 24h and 72h after transfection in T-25 flasks, exposed throughout
509 to 100 nM atropine. The experiments were performed in two biological replicates, each with two technical
510 replicates. Transfection efficiency (to the right of the chart) was monitored thanks to the mRuby2 fluorescent
511 reporter within a bicistronic cassette within each vector (see **Materials and Methods**). Significance values
512 reported in the graphs were determined by a one-tailed Student t-test, p-values: ** $0.001<p<0.01$; *
513 $0.01<p<0.05$. **D**, FRET efficiency plot of the interaction between M_2tail(368-466)-mTurquoise2 and
514 F_0F_1ATP Synthetase (CV-mCitrine), COX8a(pMito)-mCitrine and SMAC-mCitrine, as determined by
515 acceptor photobleaching measurement in a confocal microscope. Each dot represents a ROI within a cell.
516 At least 3 cells from two separate transfections were imaged for each pair.
517

518 These functional data are further supported by Fluorescence Resonance Energy Transfer (FRET)
519 data aimed at investigating the molecular interactions of the mTurquoise2 labeled M_2tail(368-466)
520 with mitochondrial proteins. Based on the oxygen consumption data (**Fig. 6A** and **Fig. S10A**) we
521 chose as primary target the F_0F_1 ATP Synthetase complex, also indicated as complex V (CV), and
522 we labeled the γ subunit with mCitrine, a fluorescent acceptor. The γ subunit is located towards
523 the mitochondrial matrix. We further monitored interactions with an intermembrane space protein
524 (SMAC) and a protein localized to the mitochondrial matrix (COX8a), both fused to the mCitrine
525 fluorescent acceptor. As clearly illustrated in **Fig. 6D**, FRET efficiency, an indicator of molecular
526 interaction, is significantly larger for M_2tail(368-466)-CV pair than both the intermembrane space
527 SMAC and the matrix COX8a. The latter result is particularly relevant, as it indicates a specific
528 interaction of M_2tail(368-466) with CV.
529

530 **Relevance of C-terminal expression and mitochondrial translocation in a physiological,**
531 **endogenous setting**

532 The results provided in the previous sections convincingly demonstrate the cap-independent
533 translation of the M_2 C-terminal fragment, its upregulation and mitochondrial localization upon
534 stress response, and the subsequent effect in regulating oxidative phosphorylation by a direct
535 interaction with complex CV of the respiratory chain. To test the physiological relevance of these
536 findings we first prepared protein extracts from heart, brain and spleen tissues from a line of knock-
537 in mice (see **Materials and Methods**), designed to have expression of a Chrm2/tdtomato fusion
538 protein driven by the endogenous M_2 muscarinic acetylcholine receptor promoter/enhancer
539 sequences. The heart and brain are known to express sizable levels of the M_2 receptor, whereas
540 the spleen, where no expression of the M_2 receptor is reported in the proteomic databases, was
541 used as a negative control.

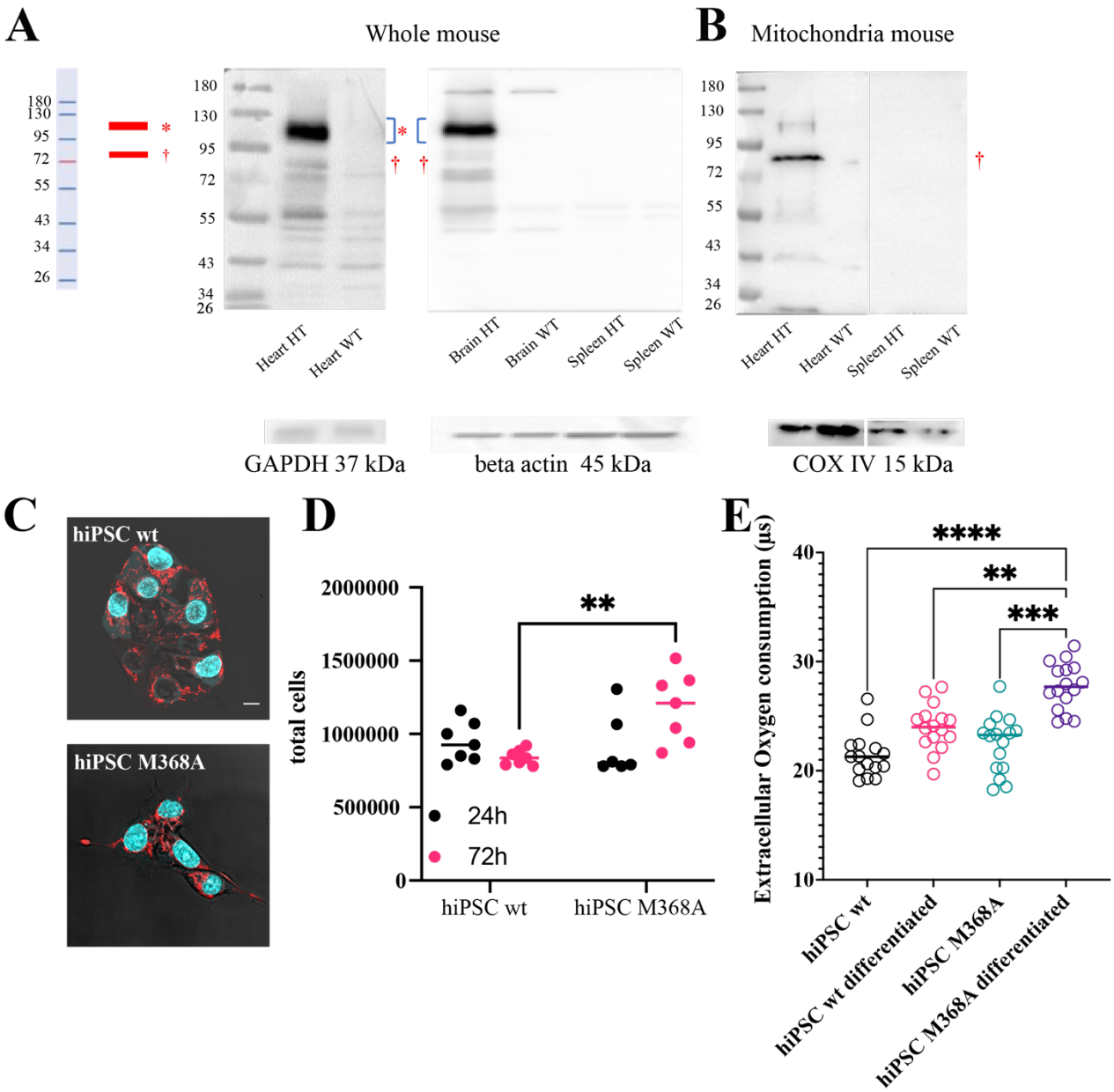

Fig. 7. IRES-mediated M_2tail(368-466) expression occurs in endogenous, physiological settings and its suppression affects cell metabolism

A, Western blot from tissue preparations originating from the indicated organs of M_2-tdtomato knock-in mice (HT) and wild-type animals (WT). Immunodetection was performed using an anti-tdtomato primary antibody. Loading control normalization was performed using GAPDH in the heart, and β-actin in the brain and spleen. **B**, Western blot (8% TRIS-Glycine PAA gel) of mitochondria purified from tissue preparations originating from the indicated organs of M_2-tdtomato knock-in mice (HT) and wild-type animals (WT), detected using an anti-tdtomato antibody. **C,** Confocal micrographs of wt hiPSCs (left) and Crispr/Cas9 clone harboring the M368A mutation within the M_2 gene (right), stained with DAPI (cyan) and Mitotracker (red). **D**, Cell proliferation assay performed for wt hiPSCs and M368A hiPSCs grown in T25 flasks., exposed

553 to Atropine. Cells were counted 24h and 72h after seeding. Significance values reported in the graphs were
554 determined by a one-tailed Student t-test, p-values: ** 0.001<p<0.01. **E**, Extracellular oxygen consumption
555 assay, performed on wt and M368A hiPSCs, prior to and after 7 days undirected differentiation under
556 Atropine exposure. The lifetime of a commercial dye increases as oxygen in the medium is progressively
557 consumed by the cells. The data displayed wascollected after 60 minutes incubation. Significance values
558 reported in the graphs were determined by a one-tailed Student t-test, p-values: *** 0.0001<p<0.001; **
559 0.001<p<0.01.

560

561 The use of a transgene tag was necessary, since antibody against the M_2 receptor are notoriously
562 ineffective when targeted at the C-terminal portion of the receptor. Instead, the tdtomato
563 fluorescent protein can be targeted by a specific polyclonal antibody, as shown by the Western
564 blot displayed in **Fig. 7A**. As expected, the full-length receptor-tdtomato fusion was observed at
565 ~130 kDa (~75 kDa contributed by the receptor and ~55 kDa contributed by tdtomato). Notably
566 we observed again (both in the heart and brain, but not in the spleen) a specific band doublet, this
567 time at ~75 kDa, which corresponds to the sum of the molecular weights of the tail fragment added
568 to the molecular weight of tdtomato. When mitochondria were purified from the heart and spleen
569 of the Chrm2/tdtomato mice **Fig. 7B** the band at ~75 kDa was substantially enriched, matching
570 the expected molecular weight of the M_2tail. These data strongly suggest that the M_2tail is
571 expressed endogenously, and it is sorted to the mitochondria.
572 We finally asked the question of what the effect of would be abolishing the translocation of the M_2
573 C-terminal fragment to the mitochondria, in a physiological and entirely label-free setting. Notably,
574 human induced pluripotent stem cells (hiPSC) combined with genome editing approach are state-
575 of-the art tools to investigate the effect of gene mutations in physiological and label-free setting.
576 Therefore, we incorporated by Crispr/Cas9 the homozygous M368A mutation in hiPSCs
577 (**Materials and Methods**). Based on our data of (**Fig. 3C**), this mutation should be sufficient to
578 significantly impair the M_2tail production and mitochondrial translocation. Wild type (wt) and
579 M368A hiPSCs were cultured in pluripotency maintaining medium, and subsequently undirectedly
580 differentiated upon exposure for seven days to DMEM-F12 medium, as described in the **Materials**
581 **and Methods**. **Fig. 7C** shows confocal micrographs for wild type and M368A hiPSCs cultured in
582 E8 medium respectively, with the M368A hiPSCs displaying a mildly more spread-out phenotype.
583 We shall note here that the M_2 receptor has been found to be expressed in PSCs lines, and it has
584 been shown to play a role in stem cell differentiation [20, 21]. In this context, however, we were
585 not interested in the canonical signaling of the receptor, and all experiments were performed with
586 a saturating concentration of atropine, to block any possible effect of the canonical signaling of

587 the M_2 receptor. We then evaluated cell proliferation, observing a significant increase in the
588 proliferation of the M368A clone 72h after seeding **Fig. 7D**. The observation that cells harboring
589 the mutation that suppresses M_2tail display an increased proliferation suggests that the same
590 effect is at play here, as observed in the overexpression system (**Fig. 6C**). These results are
591 supported by extracellular oxygen consumption assays performed, for both hiPSCs and
592 differentiated hiPSCs (**Fig. 7E**): the M368A cells indeed display an accelerated oxygen
593 consumption rate, and this effect increases as the cells progressively differentiate.
594 For comparison, the assay was also carried on HEK293 overexpressing the wild type M_2 receptor
595 and the mutant M_2M368A (**Fig. S10F**). We shall further note here that signaling properties of M_2
596 M368A with respect to the wild type M_2 receptor are comparable, as displayed by pERK
597 immunoblotting as well as FRET G_i activation assays performed in cells overexpressing either the
598 wild type M_2 or the M_2 M368A (**Fig. S10 G,H**).
599

600 ## Discussion

601 Over the last 10 years, growing evidence has accumulated indicating that GPCRs can be
602 functional and signal also at cellular locations other than the plasma membrane. These locations
603 can be associated to their canonical trafficking pathways (such as sorting vesicles and
604 endosomes) [22], but also to non-canonical locations, such as the nucleus, the nuclear
605 membrane, the Golgi apparatus and the mitochondria (reviewed in Jong et al. BPJ 2018 [23]).
606 Some of these locations are surprising, since many ligands are non-membrane permeable, and it
607 is still debated how they can reach their target receptors at such intracellular locations.
608

609 Interestingly, the specific localization of these receptors appears to go hand in hand with a specific
610 function. In these cases, activation/inhibition of mitochondrially localized GPCRs have been
611 shown to specifically affect the organelle function, ranging from oxygen consumption rates to
612 Ca^{2+} handling and even to apoptosis. Notably Benárd et al. [24] showed that the CB_1R on the
613 outer mitochondrial membranes affects neuronal energy metabolism; Suofu et al. [7]
614 demonstrated that activation of the MT_1R by a mitochondrial melatonin pool can affect cytochrome
615 C release. This is particularly interesting, since cytosolic cAMP does not appear to be able to
616 activate mitochondrial PKA, and hence a mitochondrially localized GPCR signalosome appears
617 to be required to enable such downstream signaling cascade [25].
618

619 However, other non-canonical mechanisms are also possible for the regulation of mitochondrial
620 function. It is well known that GPCRs are subject to interindividual variability, arising, for example,

621 from mRNA alternative splicing (i.e. the process which allows the recombination of exons) which
622 leads to different isoforms which may present distinct signaling and localization properties[26].
623 Receptor variants with different functional and localization properties may also occur due to other
624 processes. For example, our comprehension of eukaryotic translational regulation is facing a rapid
625 expansion, as exemplified by the observation that small open reading frames (smORFs), also
626 within long non-coding RNAs (lncRNAs), are an important class of genes, oftentimes with
627 mitochondrial localization [28].
628
629 In this study, for the first time, we provide evidence that an IRES sequence drives expression of
630 a membrane receptor fragment and acts as a regulator of its expression levels and function. IRES
631 sequences are distinct regions of the mRNAs that are capable of recruiting ribosomes in the
632 proximity of an internal initiation codon and translate transcripts in a cap-independent manner[9,
633 10, 27-29]. Here, we show that an IRES sequence is located within the third intracellular loop of
634 the M_2 muscarinic receptor, where it plays a crucial role in regulating the expression of its carboxy-
635 terminal domain, which we identified as M_2tail(368-466).
636
637 We assessed the IRES-driven expression of the C-terminal fragment through a broad set of
638 constructs, meant to exclude alternative synthesis mechanisms such as stop-codon read-through,
639 and a diversified palette of techniques. Radioligand binding data (**Table 1**) pointed to the necessity
640 of the C-terminal fragment synthesis, to explain the observed downstream signaling in mutants
641 carrying a stop codon in the initial portion of the i3loop of the M_2 receptor, upstream of M368.
642 Fluorescence microscopy allowed us visualizing the production of the EGFP-tagged C-terminal
643 fragment in these receptor mutants (**Fig. 1**).
644
645 Mutagenesis of key residues within the i3 loop of the M_2 receptor allowed us to pinpoint the 3rd in-
646 frame methionine as the most likely candidate for the beginning of the cap-independent translation
647 (**Fig. 2**). This observation appears to be supported by the observation of a peak in ribosome
648 coverage around the M368 seen in ribosome profiling databases (as reviewed in Ingolia et al.
649 [30]), and particularly prominent in those from left ventricle cardiomyocytes, where M_2 receptor
650 expression is known to be abundant [31].
651
652 To our surprise, in contrast to the plasma membrane localization of the wild type, full length M_2
653 receptor, the C-terminal fragment was localized mostly in mitochondria in HEK293 cells. This
654 localization occurred markedly when overexpressing the C-terminal fragment M_2tail(368-466), but

655 could be also clearly detected when the C-terminal fragment was expressed under the control of
656 the IRES sequence of the full-length receptor (**Fig. 3**). These results were further validated in a
657 rat cardiomyoblast cell line such as H9c2 (**Fig. S7C**).
658
659 We devised several strategies to detect the localization of the IRES-driven fragment in the
660 mitochondria by avoiding the cell-wide background signal from the full-length receptor. **Fig. 3D,E**
661 show two prominent examples, namely relying on spectrally unmixing the two components, or by
662 sending out of frame the EGFP at the C-terminus of the full-length receptor. By studying
663 mitochondria purified from HEK293 cells we could confirm that the mutation of the M368, which
664 we identified as the starting point of the IRES-mediated translation, is sufficient to suppress any
665 mitochondrial targeting of the M_2 C-terminal fragment, and most likely, its synthesis altogether
666 (**Fig. 3C**).
667
668 We then addressed the mechanism of mitochondrial import of the C-terminal fragment and its
669 localization within the organelle (**Fig.4**). Our data, originating both from live cell import kinetics as
670 well as from in-vitro import into isolated mitochondria (**Fig.4A,B**), support the notion that the
671 fragment becomes rapidly imported into mitochondria following translation in the cytosol. Once
672 inside the mitochondria, it undergoes processing leading to the appearance of a lower molecular
673 weight band, observed both in Western blots from whole cell and mice tissue protein extracts, as
674 well as from purified mitochondria and in the yeast in vitro assays (**Fig. 4C**). The fragment is found
675 predominantly in a carbonate-insoluble fraction, i.e. a membrane, and it appears to form a high
676 molecular weight complex of ~180 kDa with other mitochondrial proteins (**Fig. S7D)**.
677 Fluorescence complementation assays (**Fig. 4D**) and electron microscopy (**Fig. 4E-H**) suggest
678 that the M_2 C-terminal fragment predominantly resides in the inner mitochondrial membrane, with
679 its own C-terminal domain exposed towards the matrix. Future work should clarify the precise
680 import pathway.
681
682 Under integrated stress response, namely aminoacid starvation, IRES-mediated production of the
683 C-terminal fragment was increased (**Fig. 5A-B**), with a marked increase in mitochondrial
684 localization (**Fig. 5C)**. Most importantly, our data show that mitochondrial oxygen consumption
685 was reduced by the M_2tail(368-466) (**Fig. 6A,B**), and also cell proliferation was affected (**Fig. 6C**).
686 On these bases, the M_2tail might be needed in mitochondria as a means to reduce mitochondrial
687 basal oxygen consumption and ATP-linked respiration. An important consequence of reduced

respiration is the lower level of ROS produced in mitochondria, as we observed in agreement with this hypothesis **Fig. 6B**.

This observation was confirmed in physiological conditions by Western blots in a knock-in mice carrying a tag at the C-terminus of the endogenous M_2 receptor. These could show mitochondrial enrichment of a band corresponding to the molecular weight of the C-terminal domain (**Fig. 7A**). Moreover, the physiological relevance of our observations was tested in an entirely label-free assay, by Crispr/Cas9 editing of pluripotent stem cells in order to suppress the synthesis of the M_2 C-terminal fragment. By mutating the IRES starting methionine M368, we observed an increase of cell proliferation of this clone compared to its wild type counterpart, together with an increase of oxygen consumption rates (**Fig. 7B-D**). Overall this corroborates our hypothesis that the M_2 C-terminal fragment reduces oxygen consumption upon reaching the mitochondria. The effect was further amplified when the cells were undirectedly differentiated, and it was consistent with the shift of the cell phenotype towards oxidative phosphorylation [32].

The mechanism by which the M_2tail(368-466) may reduce oxygen consumption in mitochondria and its meaning needs to be further explored. Our FRET data (**Fig. 6D**) indicate clearly that the M_2 C-terminal fragment has a specific interaction with the F_0F_1 ATP-synthase complex, supporting the concept that it inhibits the activity of this enzyme, thus leading to the observed reduction in oxygen consumption rates. Future work should clarify the precise import pathway and the inhibitory effect of M_2tail(368-466) on F_0F_1 ATP-synthase. Nonetheless, since ROS production is implicated in the pathogenesis of several diseases [32], we would propose the hypothesis that increased localization of the M_2 C-terminal fragment in mitochondria, as it occurs under integrated stress response, might have protective effects (**Fig. 8**).

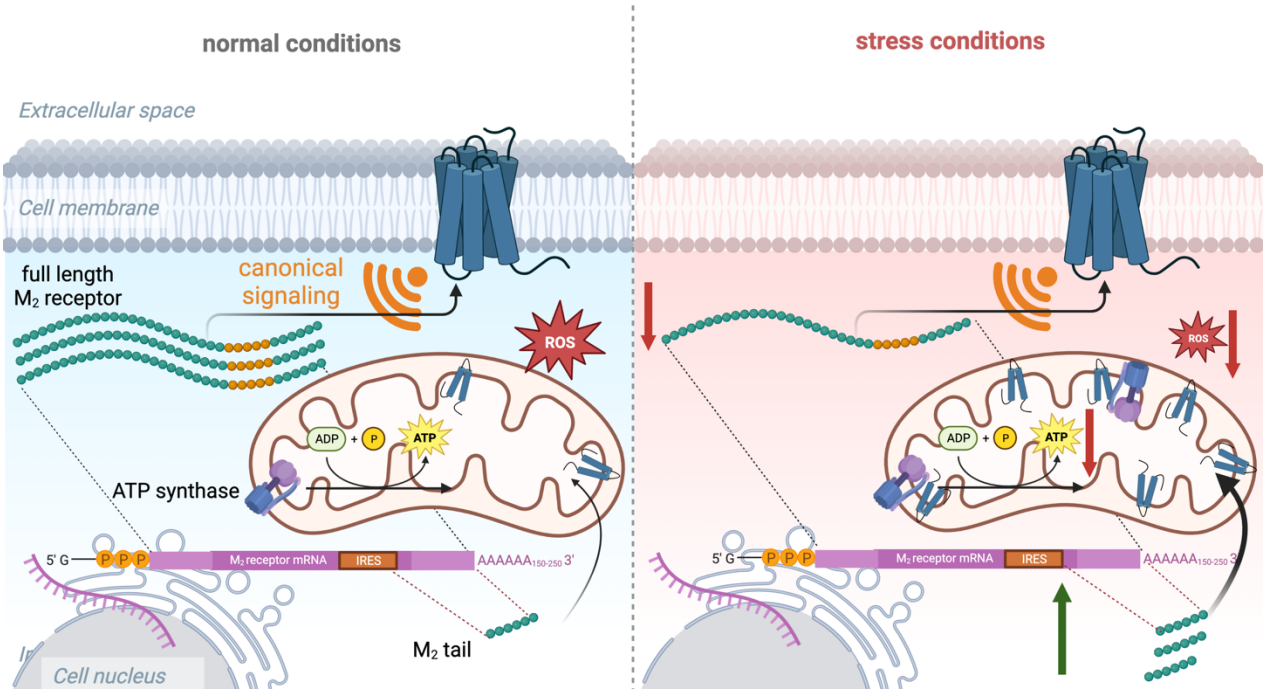

Fig. 8. Schematic representation of the wild type M_2 receptor gene products, their destination in the cell and their function.

The M_2 receptor gene gives rise to one transcript but two different translation outputs: when translation starts from the canonical cap site the wild type M2 receptor is generated (full length M_2 receptor). When translation is driven by the internal ribosome entry site (IRES) the C-terminal fragment is generated (M_2 tail). The two proteins are then sorted in two different cell compartments where they play completely different roles: the M_2 receptor signals canonically at the plasma membrane as a G protein-coupled receptor. The M_2tail is instead sorted to the mitochondria.

In normal conditions the activity of the IRES is low, and only a small amount of M_2tail is produced in the cell (left). However, upon cell stress conditions (right), M_2tail IRES-mediated translation is upregulated and M_2tail in the mitochondria interacts with the ATP synthase and reduces oxidative phosphorylation and ROS formation. Created with BioRender.

In broader terms, protection of mitochondria by unconventional import mechanisms to allow localization within the organelle of specific proteins has been previously observed for cells that undergo stress conditions[33] . The mechanism of IRES-dependent modulation of translation and consequent mitochondrial targeting of the translation product of a GPCR may provide another means, completely unrelated to the canonical signaling function of this class of membrane receptors, of a generic cellular response to overcome different types of stress by modulating the mitochondrial proteome and adjusting the mitochondrial bioenergetic state.

734

735 ## Materials and Methods

736

737 **Generation of mutant muscarinic M_2 receptors for radioligand binding studies,**
738 **Western blotting, immunohistochemistry and fluorescence microscopy**

739 Multiple receptor mutants were constructed starting from the human M_2 muscarinic receptor
740 expressed in the pcD vector [34]. The constructs are sketched in **Fig. S3** and their cloning
741 is described in detail in the **Supplementary Methods**.

742

743 **Reverse transcription**

744 Reverse transcription was performed using a 24-nucleotide antisense oligo
745 (TTACCTTGTAGCGCCTATGTTCTT) directed against the last 24 nucleotides at the 3' end
746 of the M_2 open reading frame. cDNA amplification was carried out with the same antisense
747 oligo used for reverse transcription, together with a 24 nucleotides sense oligo
748 (ATGAATAACTCAACAAACTCCTCT) directed against the first 24 nucleotides at the 5' end
749 of the M_2 open reading frame.

750

751 **Cell culture and transfection**

752 COS-7 (African green monkey kidney fibroblast-like SV40 transformed cell line) and CHO
753 (Chinese Hamster Ovary) cells (from American Type Culture Collection) were grown at 5%
754 CO_2 and 37 °C, in high glucose Dulbecco's modified Eagle's medium (DMEM)
755 supplemented with 10% fetal bovine serum (FBS), 2 mM L-glutamine, 50 IU/ml penicillin,
756 and 50 mg/ml streptomycin, and non-essential amino acids. HeLa cells (from American
757 Type Culture Collection) were cultured in the same medium, but with the double amount of
758 L-glutamine. SHSY-5Y cells were cultured in Roswell Park Memorial Institute (RPMI)
759 medium supplemented with 10% FBS, 2 mM L-glutamine, 50 IU/ml penicillin, and 50 mg/ml
760 streptomycin. Media and reagents used for cell cultures were from Euroclone, PAN Biotech,
761 Biochrome and Sigma-Aldrich. Cell transfection was performed using FuGene® transfection
762 reagents (Promega) as recommended by the manufacturer. Eighty percent confluent cells
763 were washed twice with free-serum medium and the mix of FuGene and plasmid DNA was
764 added. In every experimental condition 6-8 µg of plasmid DNA per Petri (10 cm^2) were used.
765 Cells were grown for 48 h post-transfection before use. In co-transfection experiments, half
766 amount of each plasmid DNA was used.

767 HEK293 (Human Embryonic Kidney, ECACC 96121229 from Sigma-Aldrich Chemie
768 GmbH) were cultured in DMEM (Dulbecco's modified Eagle's medium PAN biotech,
769 Aidenbach, Germany), supplemented with 4.5 g/L Glucose, 2 mM L-Glutamine, 10% FCS,
770 100 units/mL penicillin and 0.1 mg/mL streptomycin and maintained at 37 °C and 5% CO_2.
771 Cells cultured in 15-cm dishes were split at a 1:36 ratio into 6-well plates containing poly-D-
772 lysine (PDL)-coated 24 mm glass coverslips. Cells were transfected using Effectene
773 transfection reagent (QIAGEN) according to the manufacturer's instructions. Cells seeded
774 on PDL-coated coverslips in 6-well plates were transfected 16 hours after seeding with 0.6
775 µg plasmid/well.
776
777 **Fluorescence microscopy**
778 Fluorescence microscopy experiments were performed either on a Leica SP5 (or SP8)
779 Confocal Microscopes, using HyD photon counting detectors and an Argon/Ion laser (or
780 white light laser) source for 488 nm/633 nm excitation and a solid-state diode laser (or white
781 light laser) for 561 nm excitation. A solid-state diode laser was further used for 405 nm
782 excitation. A 40x 1.3 NA objective was used, and the electronic zoom was set to achieve a
783 pixel size of 50 nm. For visualization, mitochondria of transfected cells were labelled for 30
784 minutes at 37 C with 50nM MitoTracker® Deep Red FM (Invitrogen™, Thermo Scientific).
785
786 **Ligand binding studies**
787 Cells were lysed 48 h post-transfection with ice-cold 2 mM EDTA, 1 nM Na-HEPES (pH
788 7.4), scraped with a rubber policeman in the presence of ~4 ml rinsing medium, and
789 homogenized with a Polytron homogenizer (ULTRA-TURRAX) in binding assay buffer (50
790 mM Tris-HCl, pH 7.4, 155 mM NaCl, 0.01 mg/ml bovine serum albumin). Radioligand
791 bindings were carried out at 37 °C for 3 h in a final volume of 1 ml. Non-specific binding was
792 determined in presence of 1 µM atropine. For competition binding assays, increasing
793 concentrations of carbachol (from 0.01 µM up to 10 µM) were used in presence of 200 pM
794 [^{3}H]N-Methylscopolamine ([^{3}H]NMS; 78.9 Ci/mmol; PerkinElmer).
795 The bound ligand was separated from the unbound ligand using glass-fiber filters
796 (Whatmann, GF/B) with a Brandel Cell Harvester, and filters were counted with a scintillation
797 β-counter. K_D values of [^{3}H]NMS were calculated in direct saturation experiments, whereas
798 carbachol Inibitory Concentration $(IC)_{50}$ values were calculated in competition curves,
799 against 400 pM [^{3}H]NMS, fitted to one binding models using the iterative, non-linear least-
800 squares regression analysis of OriginPro 7.5 software (OriginLab Corporation).

801 **Phosphatidylinositol Breakdown Assay**

802 Transfected COS-7 cells were incubated with myo-[^{3}H]inositol (23 Ci/mmol; PerkinElmer)
803 for 48 h. Immediately before the experiment the cells were washed twice with phosphate-
804 buffered saline and incubated for 15 min in Eagle's medium containing 10 mM LiCl and 20
805 mM HEPES. The medium was then replaced by 0.25 ml of the same medium containing
806 the experimental agents. After a 1-hour incubation at 25 °C the reaction was arrested by
807 the addition of 0.75 ml of 7.5% (w/v) ice-cold trichloroacetic acid followed by a 30-min
808 incubation on ice. The trichloroacetic acid was extracted with water-saturated diethyl ether
809 (3 × 4 ml), and levels of IP_1 determined by anion exchange chromatography.

810

811 **Adenyl Cyclase Assay**

812 COS-7 cells were transfected with plasmid(s) containing the receptor of interest plus adenyl
813 cyclase V. 24 h after transfection the cells were detached with trypsin and re-cultured in 24-
814 well plates. Following an additional period of 24 h culture, they were assayed for adenyl
815 cyclase activity. The assay was performed in triplicate**.** In brief, cells were incubated in 24-
816 well plates for 2 h with 0.25 ml/well of fresh growth medium containing 5 μCi/ml [^{3}H]adenine
817 (PerkinElmer). The medium was then replaced with 0.5 ml/well of DMEM containing 20 mM
818 HEPES, pH 7.4, 0.1 mg of bovine serum albumin, and the phosphodiesterase inhibitors 1-
819 methyl-3-isobutylxanthine (0.5 mM) and Ro-20–1724 (0.5 mM). AC activity was stimulated
820 by the addition of 1 μM forskolin in the presence or absence of carbachol. After 10 min of
821 incubation at +30 °C the medium was removed, and the reaction terminated by addition of
822 perchloric acid containing 0.1 mM unlabeled cAMP followed by neutralization with KOH.
823 The amount of [^{3}H]cAMP formed under these conditions was determined by a two-step
824 column separation procedure[3].

825

826 **Immunoelectron Microscopy (IEM)**

827 Samples were fixed for 3 hours at 4 °C with a mixture of 4% PFA and 0.05% GA in 0.1M
828 PB, pH 7.4. After rinsing in the same buffer, samples were dehydrated in a graded series of
829 ethanol and embedded in medium grade LR White resin, following addition of the LR White
830 accelerator (London Resin Company, Berkshire, England). The resin was then polymerized
831 for 20 min at room temperature in tightly capped gelatine capsules. Ultrathin sections were
832 obtained using a Reichert Ultracut ultramicrotome equipped with a diamond knife and

833 collected on nickel grids. For immunogold labelling, 60-80 nm thick sections were processed
834 following the incubation protocol originally developed by Aurion (Wageningen, the
835 Netherlands). Unspecific binding was prevented by treating sections for 20 min with 0.05 M
836 glycine in PBS, at pH 7.4. A subsequent block step was made by washing sections for 30
837 min in 5% BSA, 5% normal goat serum and 0.1% cold water fish skin gelatine. Sections
838 were soaked overnight 4 °C in incubation buffer (PBS and 0.1% BSA-cTM, pH 7.4) (3x5
839 min) in a moist chamber containing the Myc-Tag (9B11) mouse antibody (Cell Signaling
840 Technology) diluted 1:50 with incubation buffer. Sections were then washed in incubation
841 buffer (6x5 min) and incubated for 1 hour with a secondary goat anti-mouse antibody
842 conjugated to 10 nm gold particles (EM Grade 10nm Goat anti-Mouse IgG Conjugate
843 EM.GAM10/1, British BioCell International, UK), diluted 1:10 in incubation buffer. After
844 rinsing in incubation buffer (6x5 min), grids were washed in PBS (6x5 min). Sections were
845 subsequently stained with uranyl acetate and observed with a Jeol JEM EXII Transmission
846 Electron Microscope at 100kV. Micrographs were acquired by the Olympus SIS VELETA
847 CCD camera equipped the iTEM software. Control sections were obtained by omitting the
848 primary antibody from the incubation mixture.
849

850 **Isolation of Yeast Mitochondria**

851 Mitochondria were isolated as in Kritsiligkou et al.[33], , 2017. In short, D273-10B yeast
852 were grown to OD600 1 in yeast peptone lactate. Cells were pelleted by centrifugation
853 (3,000g) and washed in ddH2O and the cell pellet weight was calculated. The yeast cells
854 were then washed in 100mM Tris-SO4 pH 9.4, 10mM DTT for 30 minutes in the presence
855 of constant agitation (120rpm). The cells were washed in sorbitol buffer (1.2M Sorbitol,
856 10mM KPi pH 7.4) followed by resuspension in sorbitol buffer (5ml/g of cells) supplemented
857 with zymolyase 20T (3.5mg/g of cells) and incubation for 45 minutes under constant
858 agitation (120rpm) to create spheroplasts. The spheroplasts created in this process were

859 washed in sorbitol buffer and resuspended in breaking buffer pH6.0(BB pH6.0) (600mM
860 Sorbitol buffer, 20mM MES-KOH pH 6.0, 1mM PMSF). The spheroplasts were the broken
861 in BB pH6.0 using a glass type B pestle homogeniser for 15 strokes on ice. The cell debris
862 was removed via differential centrifugation; first low speed centrifugation (1,480g 4ºC) then
863 high speed (12,000g 4 ºC). Crude mitochondria were then purified further via gradient
864 centrifugation on a 14.5-20% Nycodenz® gradient and spun at 202,496g at 4 ºC. The pure
865 mitochondria were collected with a 19-gauge needle, washed in BB pH 7.4 (600mM sorbitol
866 buffer, 20mM HEPES-KOH pH7.4) and protein concentration estimated. Finally, the
867 mitochondria are frozen at -80ºC at a concentration of 20mg/ml in BB pH 7.4 supplemented
868 with 10mg/ml fatty-acid free BSA.
869

870 **Import of M_2 receptor and M_2tail(368-466) in isolated yeast mitochondria**

871 The M_2 receptor and M_2tail(368-466) were cloned into the pSP64 in vitro translation vector
872 and translated with a 35S radiolabelled methionine label using the TNT® coupled
873 reticulocyte lysate system (Promega) following manufacturers guidelines. Each import
874 reaction comprised of 50µg of isolated yeast mitochondria resuspended in 100µl import
875 buffer 1X (600mM Sorbitol, 2mM KH2PO4, 50mM KCl, 50mM HEPES-KOH pH 7.4, 10mM
876 MgCl2, 2.5mM Na2EDTA pH 7, 5mM L-methionine, 1mg/ml fatty acid free BSA)
877 supplemented with 2mM ATP and 2.5mM NADH. 5µl of TNT translated protein was added
878 to each import reaction and the samples were incubated at 30ºC for 5,10 or 30 minutes.
879 Import was ceased by the transfer of samples on ice. Where indicated, samples were
880 treated with 0.1mg/ml Trypsin in breaking buffer (600mM Sorbitol, 20mM HEPES-KOH pH
881 7.4) for 30 minutes on ice followed by protease inactivation with the addition of soybean
882 trypsin inhibitor (SBTI)(1mg/ml) for 10 minutes. Mitochondria were reisolated by
883 centrifugation (16,000g, 4ºC) and resuspended in either 2X Laemmli sample buffer (65mM
884 Tris-HCl pH 6.8, 25% [v/v] glycerol, 2% SDS, 0.01% bromophenol blue) for SDS-PAGE

885 analysis or solubilization buffer (0.1mM EDTA, 50mM NaCl, 10% [v/v] glycerol, 20mM Tris-
886 HCl pH 7.4, 1% [w/v] digitonin) for Blue Native-PAGE analysis. For NaCO3 extraction 100µg
887 of mitochondria were pelleted after SBTI at 16,000g, 4ºC and resuspended in 200ul of 0.1M
888 NaCO3 for 30 minutes on ice followed by ultracentrifugation (100,000g 30 minutes 4ºC).
889 Supernatants were TCA-precipitated (10% [v/v] final) for 20 minutes on ice followed by
890 centrifugation (16,000g, 4ºC, 20 minutes). The TCA precipitated supernatant and the pellet
891 after ultracentrifugation were resuspended in 2X Laemmli sample buffer and proteins were
892 separated by SDS-PAGE.
893
894 **Animal Experiments**
895 All animal experiments were carried out according to the German animal welfare act,
896 considering the guidelines of the National Institute of Health and the 2010/63/EU Directive
897 of the European Parliament on the protection of animals used for scientific purposes. The
898 animals had free access to food and water and were kept in individually ventilated cages
899 under a 12h:12h light/dark regime (light from 6:30 am to 6:30 pm), a constant 22±2°C
900 temperature and 55±10% humidity.
901 The transgenic line B6.Cg-Chrm2tm1.1Hze/J, also known as Chrm2-tdT-D knock-in, was
902 obtained from 'The Jackson Laboratory' (Stock No: 030330). They are heterozygous
903 animals, designed to have expression of a Chrm2/tdTomato fusion protein directed by the
904 endogenous M2 muscarinic acetylcholine receptor promoter/enhancer sequences.
905
906 **Tissue preparation and immunoblot of endogenous M_2 receptor in Chrm2-tdT-D**
907 **knock-in mice**
908 Mouse tissues were weighed out and ice-cold lysis buffer was added to approx. 0.2-0.5mg
909 tissue/ml buffer (10mM K2HPO4, 150mM NaCl, 5mM EDTA, 5mM EGTA, 1% Triton X-100,
910 0.2% Na-deoxycholate. Fresh protease inhibitors PMSF 0.5mM, Na3VO4 0.1mM, NaF
911 50mM, Jenny's mix (Soybean trypsin inhibitor 3.2µg/ml, Aprotinin 2µg/ml, Benzamidin
912 0.5mM) were added to the buffer.
913 Samples were first homogenized, and then pellet debris were centrifuged at 4°C for 30
914 minutes at max speed (tabletop) and the supernatant (soluble proteins) was transferred into
915 fresh tube (pellets = non-soluble proteins)

916 Protein concentrations were determined with BCA assay. Cell lysates were loaded using
917 Laemmli Buffer 2x (Sigma Aldrich) in equal mass (see above for the immunoblot procedure)
918 into 8% polyacrylamide gels.
919 The membrane was then incubated overnight at 4 °C with primary antibody solution (1:1000
920 anti β-actin (13E5) rabbit primary antibody #4970 from Cell Signaling) (1:1000 anti GAPDH)
921 (1:1000 anti-TdTomato rabbit primary antibody #632496 from Takara).
922
923 **Isolation of mitochondrial fractions and immunodetection**
924 HEK293 cells were seeded in 15 cm plates and transfected after 24h according to
925 manufacturer protocols (Effectene, Qiagen) using 5 µg of plasmid DNA. 48h after
926 transfection cells were harvested and centrifuged at 1000 rpm for 10 minutes, resuspended
927 in NaCl 0.9% (w/v) and centrifuged at 1000 rpm for 10 minutes.
928
929 Mouse tissues were freshly excised and placed in ice cold PBS (1x). The samples were
930 washed with NaCl 0.9% (w/v). The homogenization steps were performed with Precellys
931 Evolution Homogenizer, at 4500 rpm for 10 seconds.
932 The samples were processed according to manufacturer protocols (Qproteome
933 Mitochondria Isolation Kit, Qiagen). From the different steps were obtained three different
934 fractions: the cytosolic, the microsomal and the mitochondrial fraction.
935 The fresh mitochondrial pellet was resuspended in 150µL of ice-cold lysis buffer and the
936 protein concentration of the three fractions from each sample was quantified with a BCA
937 assay (see above).
938 Cell lysates were loaded into 12% polyacrylamide gels using an SDS loading buffer (6x
939 solution: 2.28g Tris-HCl, 2.313 DTT, 6g SDS, 30% Glycerol and 0.03% bromophenol blue
940 in a final volume of 50 mL) in equal mass (see above for the immunoblot procedure).
941 The membrane was then incubated overnight at 4 °C with primary antibody solution using
942 the following concentrations: 1:1000 anti β-actin (13E5) rabbit primary antibody (#4970 from
943 Cell Signaling), 1:1000 anti-tdtomato rabbit primary antibody (#632496 from Takara),
944 1:1000 anti β-tubulin mouse primary antibody, 1:1000 anti GAPDH mouse primary antibody,
945 1:1000 anti COXIV mouse primary antibody (#ab33985 from abcam).
946
947 **Quantification of M_2tail(368-466) mitochondrial import kinetics from confocal time**
948 **sequences** Before imaging, 2.5×10^4 HEK-TSA cells were seeded in each PDL-coated well
949 of the µ-Slide 8 well (Ibidi) with DMEM (ScienCell™) supplemented with 10% FBS and 1%

950 P/S overnight, and transfected with a total of 2 μg C-terminal EGFP tagged M_2 tail using
951 Lipofectamine 2000 (Thermo Fisher Scientific) according to the manufacturer protocol after
952 washing with 200 μL PBS and refreshing with 100 μL DMEM (ScienCell™) supplemented
953 with 10% FBS and 1% P/S. After transfection for five hours, mitochondria of transfected
954 cells were rapidly labelled with 50nM MitoTracker® Deep Red FM (Invitrogen™, Thermo
955 Scientific) in FluoroBrite DMEM medium (Thermo Scientific) supplemented with 1% P/S for
956 20 minutes after the removal of old culture medium. After mitochondria labeling, the μ-Slide
957 were washed twice with FluoroBrite DMEM medium (Thermo Scientific) and subsequently
958 mounted onto the TCS SP8 confocal microscope (Leica) (See imaging). Firstly, the stage
959 of the microscope was equilibrated in temperature, and the acquisition mode was set to the
960 tile scanning. After storing the position of each desired transfected cells, the imaging mode
961 was set to XYT and a HC PL APO CS2 40×/NA1.3 oil immersion objective was selected.
962 Both DIC channel and HyD were utilized to obtain 512×512 pixels images. Laser
963 wavelengths were set as described in the section Fluorescence Microscopy above. All
964 settings remained the same throughout the whole measurement. Images were taken at
965 every 30 minutes over a 5h interval. The images were afterwards analyzed by ImageJ
966 software, using the Plugin 'JACoP'. Briefly, the degree of colocalization between EGFP-
967 tagged M_2tail(368-466) (CH1) and MitoTracker stained mitochondria (CH2) was quantified
968 by Mander's colocalization coefficients (40) [38]. The two colocalization coefficients M1
969 ($M1 = \frac{CHB}{CH1}$) and M2 ($M2 = \frac{CHB}{CH2}$), CHB indicates overlapping pixels in channel 1 and channel
970 2. A threshold was determined for individual channel in order to distinguish specific signals
971 from nonspecific ones. Due to their sensitivities to thresholds, the Pearson correlation
972 coefficient (PCC)[35, 36] , as well as the faster decaying attribute of nonspecific signals,
973 were also taken into account while estimating thresholds for each channel. For the analysis
974 of each cell, the threshold for Mitotracker channel was kept constant. Whereas the threshold
975 for EGFP channel was evaluated based on the PCC value.
976

977 **Transfection and expression of split-GFP constructs in HEK293 cells**

978 To perform the sequential split GFP complementation assay illustrated in **Figs 4D and 5C-**
979 **D**, 3×10^5 HEK-TSA cells were seeded on a 10% poly-D-lysine (PDL)-coated 25mm
980 coverslip in each well of a Falcon® 6-well flat-bottom plate (StemCell™) and cultured
981 overnight. Cells were transfected using Effectene (see above) with a 0.4 μg Mito-GFP1-10
982 plasmid. The cells were then washed once with fresh 2 mL phosphate-buffered saline (PBS)
983 first and supplemented with 1.5 mL fresh DMEM medium (ScienCell™) supplemented with

984 10% FBS and 1% P/S. After adding the transfection mixture, the cells were cultured
985 overnight. After the first transfection, a second transfection of a 0.6 µg plasmid encoding
986 either the C-terminal GFP11 tagged M_2tail(368-466) or M_2 receptor was performed using
987 the Effectene Transfection Reagent (Qiagen). After washing each well with 2 mL PBS, the
988 old medium was exchanged with 1.5 mL low glucose Minimum Essential Medium (MEM)
989 (Gibco™, Thermo Scientific) supplemented with 1% P/S, in order to create a stress-like cell
990 starvation condition. After a four hours starvation, the cells were fixed using 4%
991 polyformaldehyde (PFA)/PBS at 37℃ for 30 minutes and washed twice with PBS before
992 imaging.
993
994 **Oxygen consumption measured with the Seahorse assay**
995 $5x10^4$ COS7 cells were seeded in seahorse 24MW plates with Complete media (DMEM
996 supplemented with 10%FBS and 1X PS) and then incubated for about 4h at 37C in a cell
997 incubator. After this incubation, cells were washed twice with Seahorse media
998 supplemented with glutamate (1 mM), pyruvate (1 mM) and glucose (20 mM) and then
999 incubated for 1h at 37 °C in an incubator without CO2 before being analyzed in the
1000 Seahorse XF Analyzers. In particular, the baseline cell oxygen consumption rate (OCR) was
1001 measured at the beginning of the assay, followed by measurements of ATP linked
1002 respiration and maximal respiratory capacity after the addition of respectively oligomycine
1003 (1 µM) and the FCCP protonophore (1 µM). Finally, rotenone (1 µM), an inhibitor of complex
1004 I, and antimycin (1 µM), inhibitor of complex III, were added to shut down completely the
1005 electron transport chain (ETC) function, revealing the non-mitochondrial respiration.
1006
1007 **Extracellular oxygen consumption**
1008 HEK293 cells 24h after transfection and hPSCs were harvested and seeded respectively in
1009 96 multiwell black plate and pre-coated (Geltrex A1413302, Thermo Fisher) 96 multiwell
1010 black plate, $5x10^4$ cells for well; after incubation O/N at 37 °C and in 5% CO2, the cell culture
1011 medium was replaced by HBSS and the assay were performed according to the
1012 manufacturer protocols (abcam Extracellular Oxygen Consumption Assay).
1013
1014 **Generation of M368A hiPSC clone**
1015 The human induced pluripotent stem cell (hiPSC) line BIHi005-A (https://hpscreg.eu/cell-
1016 line/BIHi005-A) was used to generate an isogenic iPSC clone (BIHi005-A-39) with M368A
1017 mutation using a protocol previously described (42) [40]. In brief, small guide RNA (sgRNA)

1018 targeting the M_2 gene close to the mutation site to be corrected were designed using the
1019 http://crispor.tefor.net/ webpage and the sgRNA (5`- AGTCATCTTCACAATCTTGC-3`)
1020 were synthesized by Integrated DNA technologies (https://eu.idtdna.com). The donor
1021 ssODN template was designed to convert the ATG to GCT and was synthesized as an
1022 Ultramar DNA oligo by IDT. (5´-
1023 AAAAGTGACTCATGTACCCCAACTAATACCACCGTGGAGGTAGTGGGGTCTTCAGGT
1024 CAGAATGGAGATGAAAAGCAGAATATTGTAGCCCGCAAGATTGTGAAGGCTACTAAG
1025 CAGCCTGCAAAA-3´). The Ribonucleoprotein (RNP) complexes were prepared by
1026 incubating of 1.5µg Cas-9 protein and 360 ng gRNA for 10 minutes at room temperature.
1027 For delivery of RNPs and ssODN template, 10µl cell suspension containing Cas9 RNPs and
1028 ssODN and 1x105 cells were electroporated using the Neon transfection System
1029 (ThermoFisher Scientific). The electroporated cells were plated in one well of 6 well plate
1030 with StemFlex media (ThermoFisher Scientific) supplemented CloneR™ (Stemcell
1031 technologies). Three days after the transfection we analyzed the bulk population using the
1032 Sanger sequencing to estimate the editing efficiency. Thereafter, the automated single cell
1033 cloning of the genome edited cell pool was performed as described in protocol [37] . The
1034 clones were screened by SANGER sequencing. The positive confirmed clones were
1035 banked and characterized for pluripotency and karyotype stability as described in [38] .
1036 Briefly, for pluripotency assay, single cells were labelled with conjugated antibodies.
1037 Surface markers (SSEA1, SSEA4 and TRA1-60) staining was performed in unfixed cells by
1038 incubation with antibodies diluted in 0.5% BSA/PBS (10 min, 4 °C, dark). Intracellular
1039 markers (OCT3/4, NANOG) were stained by fixation/permeabilization solution (Miltenyi
1040 Biotec, 130-093-142) (30 min, 4 °C, dark) followed by antibody incubation in
1041 permeabilization buffer (Miltenyi Biotec) (30 min, 4 °C, dark). Analysis was done using the
1042 MACSQuant® AnalyzerVYB and FlowJo v10.4.
1043 Briefly, for karyotype stability, genomic DNA was isolated using the DNeasy blood and
1044 tissue kit (Qiagen, Valencia, CA, United States) and samples were analyzed using the
1045 human Illumina OMNI-EXPRESS-8v1.6 BeadChip. First, the genotyping was analyzed
1046 using GenomeStudio 1 genotyping module (Illumina). Thereafter, KaryoStudio 1.3 (Illumina)
1047 was used to perform automatic normalization and to identify genomic aberrations utilizing
1048 settings to generate B-allele frequency and smoothened Log R ratio plots for detected
1049 regions. The stringency parameters used to detect copy number variations (CNVs) were set
1050 to 75 kb (loss), 100 kb (gain) and CN-LOH (loss of heterozygosity) regions larger than 3
1051 MB.

1052

1053 **Culture and handling of hiPSCs cells**

1054 hiPSCs were cultured on Geltrex (Thermo Fisher) coated plates using: Essential 8 medium
1055 (Thermo Fisher). The culture was routinely monitored for mycoplasma contamination using
1056 a PCR assay. 10 μM ROCK Inhibitor Y-27632 2HCl (Selleck Chemicals, #SEL-S1049) was
1057 added after cell splitting to promote survival. hiPSC cultures were kept in a humidified
1058 atmosphere of 5% CO2 at 37°C and 5% oxygen. hiPSCs were undirectedly differentiated
1059 to a mixture of three lineages (ectodermal, endodermal and mesodermal) by replacing
1060 Essential 8 medium with DMEM-F12 medium supplemented with 10% FBS for seven days.
1061 10 μM ROCK Inhibitor Y-27632 2HCl (Selleck Chemicals) was added after cell splitting to
1062 promote survival.

1063

1064 **Cell proliferation assay with HEK293 cells**

1065 $4x10^5$ HEK293 cells 24h after transfection and $4x10^5$ hPSCs were seeded respectively in
1066 T25 flask and pre-coated T25 flask, in culture medium with Atropine at final concentration
1067 of 100nM; the medium with Atropine was replaced every day. After 72h from transfection of
1068 the HEK293 and from seeding of the hiPSCs, the medium and the cells were collected and
1069 centrifuged, the pellet was resuspended in the same amount of medium for each pellet; an
1070 aliquot of the resuspension was mixed with the same amount of Trypan blue (ratio 1:1), 10
1071 microliters were used for counting in a Neubauer chamber.

1072

1073 **Fluorescence plate reader assays**

1074 HEK293 cells were grown on 6 well plates without coverslips, and, upon reaching 60-70%
1075 confluence, the cells were transfected using Effectene (Quiagen, Venlo Netherlands)
1076 according to the manufacturer's instructions. After 24 h the cells were split and transferred
1077 to 96 well (black plate) at a seeding density of 50,000 cells/well. The 96 well plate was pre-
1078 coated with Poly-D-Lysine for 30 min at RT. The medium was removed and each well was
1079 washed 3x with 100μl HBSS. The cells were finally analyzed by a fluorescence plate reader
1080 (Neo2, BioTek, Bad Friedrichshall) in HBSS.

1081

1082

1083 **Statistical analysis**

1084 Significance values reported in the graphs, in comparing tabulated values, were determined
1085 by a one-tailed Student t-test using Prism 9 (GraphPad Software), and significance values

(p-values) are indicated according to the following legend: **** $p<0.0001$; *** $0.0001<p<0.001$; ** $0.001<p<0.01$; * $0.01<p<0.05$. p-values larger than 0.05 are deemed non-significant. Unless otherwise indicated, bar charts and scatter plots indicate average value with s.e.m.

Acknowledgments

We are grateful to Dr. Marco Marcia (EMBL) for insightful discussion. I.P acknowledges a short term exchange grant from the Deutscher Akademischer Austauschdienst (DAAD). F.P. Acknowledges support from the University of L'Aquila towards international mobility.

Funding:

European Union's Horizon2020 Marie Skłodowska-Curie Actions (MSCA) Program under Grant Agreement 641833 (ONCORNET). This project was funded by the Deutsche Forschungsgemeinschaft (DFG, German Research Foundation) through Project 421152132 SFB1423 subproject C03 (P.A. and M.J.L.)

Author contributions:

Conduced primary experiments: FP, IF, PA, ZW, MR, IP, RE, HZ, UZ, MET, JDG, SS, ART, SA, MC

Contributed to the experimental data: MG, CP, GA, FM, BP, AR, EC

Contributed tools and reagents: NT and SD

Contributed to experimental design and assisted in writing paper: PA, IP, IF, MR, UZ, AT, KT, VF, FA, FG, MS

Conceived and lead the study, and wrote the paper: PA, MJL and RM

Competing interests:

The authors declare that they have no conflicts of interest with the contents of this article.

Data and materials availability:

Source data will be provided with this manuscript.

References

1. Kruse AC, Kobilka BK, Gautam D, Sexton PM, Christopoulos A, Wess J. Muscarinic acetylcholine receptors: novel opportunities for drug development. Nature Reviews Drug Discovery. 2014;13(7):549-60. doi: 10.1038/nrd4295.
2. Ad F, A C, Nm N. Muscarinic Receptors. 2012 ed: Springer Berlin Heidelberg; 2012.
3. Novi F, Scarselli M, Corsini GU, Maggio R. The Paired Activation of the Two Components of the Muscarinic M3 Receptor Dimer Is Required for Induction of ERK1/2 Phosphorylation. Journal of Biological Chemistry. 2004;279(9):7476-86. doi: 10.1074/jbc.M306818200.
4. Calebiro D, Nikolaev VO, Persani L, Lohse MJ. Signaling by internalized G-protein-coupled receptors. Trends in Pharmacological Sciences. 2010;31(5):221-8. doi: 10.1016/j.tips.2010.02.002.
5. Zhang X, Bedigian AV, Wang W, Eggert US. G protein-coupled receptors participate in cytokinesis. Cytoskeleton. 2012;69(10):810-8. doi: 10.1002/cm.21055.
6. Hebert-Chatelain E, Desprez T, Serrat R, Bellocchio L, Soria-Gomez E, Busquets-Garcia A, et al. A cannabinoid link between mitochondria and memory. Nature. 2016;539(7630):555-9. doi: 10.1038/nature20127.
7. Suofu Y, Li W, Jean-Alphonse FG, Jia J, Khattar NK, Li J, et al. Dual role of mitochondria in producing melatonin and driving GPCR signaling to block cytochrome c release. Proceedings of the National Academy of Sciences. 2017;114(38). doi: 10.1073/pnas.1705768114.
8. Maggio R, Fasciani I, Rossi M, Gregorio JD, Pietrantoni I, Puca V, et al. Variants of G protein-coupled receptors: a reappraisal of their role in receptor regulation. Biochemical Society Transactions. 2016;44(2):589-94. doi: 10.1042/BST20150239.
9. Jackson RJ, Kaminski A. Internal initiation of translation in eukaryotes: the picornavirus paradigm and beyond. RNA (New York, NY). 1995;1(10):985-1000.
10. Hellen CUT, Sarnow P. Internal ribosome entry sites in eukaryotic mRNA molecules. Genes & Development. 2001;15(13):1593-612. doi: 10.1101/gad.891101.
11. Popot JL, Engelman DM. Membrane protein folding and oligomerization: the two-stage model. Biochemistry. 1990;29(17):4031-7. doi: 10.1021/bi00469a001. PubMed PMID: 1694455.
12. Maggio R, Vogel Z, Wess J. Reconstitution of functional muscarinic receptors by co-expression of amino- and carboxyl-terminal receptor fragments. FEBS Letters. 1993;319(1-2):195-200. doi: 10.1016/0014-5793(93)80066-4.
13. Bathe-Peters M, Gmach P, Annibale P, Lohse MJ. Linescan microscopy data to extract diffusion coefficient of a fluorescent species using a commercial confocal microscope. Data in Brief. 2020;29:105063-. doi: 10.1016/j.dib.2019.105063.
14. Dong C, Filipeanu CM, Duvernay MT, Wu G. Regulation of G protein-coupled receptor export trafficking. Biochimica et Biophysica Acta (BBA) - Biomembranes. 2007;1768(4):853-70. doi: 10.1016/j.bbamem.2006.09.008.
15. Kamiyama D, Sekine S, Barsi-Rhyne B, Hu J, Chen B, Gilbert LA, et al. Versatile protein tagging in cells with split fluorescent protein. Nature Communications. 2016;7(1):11046-. doi: 10.1038/ncomms11046.

1164 16. Newman LE, Schiavon C, Kahn RA. Plasmids for variable expression of proteins
1165 targeted to the mitochondrial matrix or intermembrane space. Cellular Logistics.
1166 2016;6(4):e1247939-e. doi: 10.1080/21592799.2016.1247939.
1167 17. Thakor N, Holcik M. IRES-mediated translation of cellular messenger RNA
1168 operates in eIF2α- independent manner during stress. Nucleic Acids Research.
1169 2012;40(2):541-52. doi: 10.1093/nar/gkr701.
1170 18. Holcik M, Sonenberg N. Translational control in stress and apoptosis. Nature
1171 Reviews Molecular Cell Biology. 2005;6(4):318-27. doi: 10.1038/nrm1618.
1172 19. Bonfili L, Cecarini V, Cuccioloni M, Angeletti M, Flati V, Corsetti G, et al. Essential
1173 amino acid mixtures drive cancer cells to apoptosis through proteasome inhibition and
1174 autophagy activation. The FEBS Journal. 2017;284(11):1726-37. doi:
1175 10.1111/febs.14081.
1176 20. Ishizuka T, Ozawa A, Katsuura M, Nomura S, Satoh Y. Effects of muscarinic
1177 acetylcholine receptor stimulation on the differentiation of mouse induced pluripotent stem
1178 cells into neural progenitor cells. Clinical and Experimental Pharmacology and
1179 Physiology. 2018;45(11):1198-205. doi: 10.1111/1440-1681.12993.
1180 21. Hoogduijn MJ, Cheng A, Genever PG. Functional Nicotinic and Muscarinic
1181 Receptors on Mesenchymal Stem Cells. Stem Cells and Development. 2009;18(1):103-
1182 12. doi: 10.1089/scd.2008.0032.
1183 22. Weinberg ZY, Puthenveedu MA. Regulation of G protein-coupled receptor
1184 signaling by plasma membrane organization and endocytosis. Traffic. 2019;20(2):121-9.
1185 doi: 10.1111/tra.12628.
1186 23. Jong Y-JI, Harmon SK, O'Malley KL. GPCR signalling from within the cell. British
1187 Journal of Pharmacology. 2018;175(21):4026-35. doi: 10.1111/bph.14023.
1188 24. Bénard G, Massa F, Puente N, Lourenço J, Bellocchio L, Soria-Gómez E, et al.
1189 Mitochondrial CB1 receptors regulate neuronal energy metabolism. Nature
1190 Neuroscience. 2012;15(4):558-64. doi: 10.1038/nn.3053.
1191 25. Lefkimmiatis K, Leronni D, Hofer AM. The inner and outer compartments of
1192 mitochondria are sites of distinct cAMP/PKA signaling dynamics. Journal of Cell Biology.
1193 2013;202(3):453-62. doi: 10.1083/jcb.201303159.
1194 26. Marti-Solano M, Crilly SE, Malinverni D, Munk C, Harris M, Pearce A, et al.
1195 Combinatorial expression of GPCR isoforms affects signalling and drug responses.
1196 Nature. 2020;587(7835):650-6. doi: 10.1038/s41586-020-2888-2.
1197 27. Pestova TV, Shatsky IN, Hellen CU. Functional dissection of eukaryotic initiation
1198 factor 4F: the 4A subunit and the central domain of the 4G subunit are sufficient to
1199 mediate internal entry of 43S preinitiation complexes. Molecular and Cellular Biology.
1200 1996;16(12):6870-8. doi: 10.1128/MCB.16.12.6870.
1201 28. Fitzgerald KD, Semler BL. Bridging IRES elements in mRNAs to the eukaryotic
1202 translation apparatus. Biochimica et Biophysica Acta (BBA) - Gene Regulatory
1203 Mechanisms. 2009;1789(9-10):518-28. doi: 10.1016/j.bbagrm.2009.07.004.
1204 29. Jan E, Sarnow P. Factorless Ribosome Assembly on the Internal Ribosome Entry
1205 Site of Cricket Paralysis Virus. Journal of Molecular Biology. 2002;324(5):889-902. doi:
1206 10.1016/S0022-2836(02)01099-9.
1207 30. Ingolia NT, Hussmann JA, Weissman JS. Ribosome Profiling: Global Views of
1208 Translation. Cold Spring Harbor Perspectives in Biology. 2019;11(5):a032698-a. doi:
1209 10.1101/cshperspect.a032698.

1210 31. van Heesch S, Witte F, Schneider-Lunitz V, Schulz JF, Adami E, Faber AB, et al.
1211 The Translational Landscape of the Human Heart. Cell. 2019;178(1):242-60.e29. doi:
1212 10.1016/j.cell.2019.05.010.
1213 32. Guo C, Sun L, Chen X, Zhang D. Oxidative stress, mitochondrial damage and
1214 neurodegenerative diseases. Neural regeneration research. 2013;8(21):2003-14. doi:
1215 10.3969/j.issn.1673-5374.2013.21.009.
1216 33. Kritsiligkou P, Chatzi A, Charalampous G, Mironov A, Grant CM, Tokatlidis K.
1217 Unconventional Targeting of a Thiol Peroxidase to the Mitochondrial Intermembrane
1218 Space Facilitates Oxidative Protein Folding. Cell Reports. 2017;18(11):2729-41. doi:
1219 10.1016/j.celrep.2017.02.053.
1220 34. Bonner TI, Buckley NJ, Young AC, Brann MR. Identification of a Family of
1221 Muscarinic Acetylcholine Receptor Genes. Science. 1987;237(4814):527-32. doi:
1222 10.1126/science.3037705.
1223 35. Manders EM, Stap J, Brakenhoff GJ, van Driel R, Aten JA. Dynamics of three-
1224 dimensional replication patterns during the S-phase, analysed by double labelling of DNA
1225 and confocal microscopy. Journal of Cell Science. 1992;103(3):857-62. doi:
1226 10.1242/jcs.103.3.857.
1227 36. Manders EMM, Verbeek FJ, Aten JA. Measurement of co-localization of objects in
1228 dual-colour confocal images. Journal of Microscopy. 1993;169(3):375-82. doi:
1229 10.1111/j.1365-2818.1993.tb03313.x.
1230 37. Vallone VF, Telugu NS, Fischer I, Miller D, Schommer S, Diecke S, et al. Methods
1231 for Automated Single Cell Isolation and Sub-Cloning of Human Pluripotent Stem Cells.
1232 Current Protocols in Stem Cell Biology. 2020;55(1). doi: 10.1002/cpsc.123.
1233 38. Metzler E, Telugu N, Diecke S, Spuler S, Escobar H. Generation of two human
1234 induced pluripotent stem cell lines derived from myoblasts (MDCi014-A) and from
1235 peripheral blood mononuclear cells (MDCi014-B) from the same donor. Stem Cell
1236 Research. 2020;48:101998-. doi: 10.1016/j.scr.2020.101998.
1237